Alt, J.C., Kinoshita, H., Stokking, L.B., and Michael, P.J. (Eds.), 1996
Proceedings of the Ocean Drilling Program, Scientific Results, Vol. 148

38. *DATA REPORT:* MAGNETIC PROPERTIES AND MAGNETIC OXIDE MINERALOGY OF UPPER CRUSTAL ROCKS FROM HOLES 504B AND 896A[1]

Laura B. Stokking,[2] Elizabeth A. Heise,[2] Simon Allerton,[3] and Horst-Ulrich Worm[4]

ABSTRACT

We present the results of studies of magnetic mineralogy and magnetic properties of Holes 504B and 896A upper crustal rocks recovered during Leg 148. The ratio of saturation remanence to saturation magnetization (J_{RS}/J_S) ranges from 0.012 to 0.154 (mean = 0.06) in samples from Hole 504B, consistent with pseudo-single-domain behavior. Hole 896A samples display a variable ratio of J_{RS}/J_S that ranges from 0.012 to 0.154 (mean = 0.076), reflecting the differences in grain morphologies and magnetic properties between pillow and massive units.

Intensity of natural remanent magnetization (NRM) ranges from 0.01 to 0.24 A/m (mean = 0.09 A/m) in Hole 504B samples, less than that measured in samples recovered during other legs because the drilling-induced remanence imparted by the bottom-hole assembly was substantially less during Leg 148. Volume susceptibility averages 0.032 ± 0.029 SI, similar to that from upper parts of the dike sequence. In all samples examined from Hole 504B, high-temperature oxidation of primary titanomagnetite has produced lamellae or pods of magnetite and ilmenite. Hydrothermal alteration has further altered the minerals in some samples to a mixture of magnetite, ilmenite, titanite, and a high-titanium mineral (either rutile or anatase). Electron microprobe analyses show that magnetite lamellae are enriched in the trivalent oxides Cr_2O_3 (mean = 0.076 wt%), Al_2O_3 (mean = 0.566 wt%), and V_2O_3 (mean = 0.757 wt%), whereas divalent oxides are concentrated in ilmenite lamellae (mean MnO = 1.997 wt% and mean MgO = 0.073 wt%).

In samples from Hole 896A, NRM intensity ranges from 0.14 to 22.59 A/m (mean = 5.06 ± 4.91 A/m). Volume susceptibility averages 0.0272 ± 0.0254 SI. Low-temperature oxidation of primary titanomagnetite has produced titanomaghemite exhibiting shrinkage cracks. Ulvöspinel content averages 0.508 and ranges from 0.217 to 0.647. Titanomaghemite appears slightly enriched in Al_2O_3 (mean = 1.697 wt%), Cr_2O_3 (mean = 0.064 wt%), V_2O_3 (mean = 0.673 wt%), MnO (1.257 wt%), and MgO (0.577 wt%).

INTRODUCTION

During Ocean Drilling Program (ODP) Leg 148, Hole 504B was deepened from 2000 to 2111.0 m below seafloor (mbsf), and Hole 896A was cored from 195.1 to 469 mbsf (290 m into basement). Hole 504B lies 201 km south of the Costa Rica Rift (Fig. 1), the easternmost arm of the Galapagos Spreading Center in 6.6-m.y.-old crust (Cande and Kent, 1992). Hole 504B, drilled during eight Deep Sea Drilling Project (DSDP) and ODP legs, provides our most important in situ reference section for the structure of shallow ocean crust. Drilling results of previous legs to Hole 504B are summarized in CRRUST (1982); Cann, Langseth, Honnorez, Von Herzen, White, et al. (1983); Anderson, Honnorez, et al. (1982); Anderson, Honnorez, Becker, et al. (1985); Leinen, Rea, et al. (1986); Becker, Sakai, et al. (1988, 1989), Becker et al. (1989); Alt et al. (1986); Becker, Foss, et al. (1992), and Dick, Erzinger, Stokking, et al. (1992). Site 896, 1 km to the south of Site 504, was drilled to examine local variability in volcanic stratigraphy and the effects of off-axis hydrothermal activity on basement alteration in an area of high heat flow.

We present the results of studies of magnetic mineralogy and magnetic properties of upper crustal rocks from Holes 504B and 896A drilled during Leg 148. Allerton et al. (this volume) discuss the paleomagnetism of Holes 504B and 896A and Worm et al. (this volume) discuss the results of downhole magnetic logging, thermal properties of Leg 148 samples, and their implications for understanding the source of marine magnetic anomalies.

BACKGROUND

Understanding the structure, mineralogy, and chemical alteration processes in the oceanic crust are among the most important scientific goals of ODP and of Leg 148. Knowledge of the nature of the oceanic basement is derived mainly from studies of ophiolite complexes, remote geophysical surveys, and studies made on dredged or cored samples from the ocean floor. Only Hole 504B penetrates through the extrusive pillow lavas into the sheeted dike complex to provide a representative in situ section of the ocean crust.

The magnetic properties of rocks depend on many variables: the types of magnetic minerals present in the rock (which themselves reflect the initial rock composition and any alteration, thermal or chemical, that the rock has undergone), the concentrations and the grain volumes of the various magnetic minerals in the rock, and the magnetic domain state of those minerals. The predominant primary magnetic mineral in ocean crustal rocks is titanomagnetite, an inverse spinel that is a solid solution between iron- and titanium-bearing end members, which may also contain aluminum, chromium, magnesium, vanadium, manganese, and nickel. Secondary phases, such as titanomaghemite, ilmenite, magnetite, hematite, and titanite, are produced by thermal and chemical alteration of titanomagnetite. In some cases, secondary phases and alteration textures, that is, the exsolution of primary titanomagnetite into low-titanium titanomagnetite and high-titanium hemoilmenite (Haggerty, 1976; Smith et al., 1991), can be observed using reflected light microscopy (Ade-Hall et al., 1971; Johnson and Hall, 1978) or backscattered electron imaging in conjunction with electron microprobe analysis. In other cases, however, the exsolution lamellae are too fine to be observed optically but may

[1] Alt, J.C., Kinoshita, H., Stokking, L.B., and Michael, P.J. (Eds.), 1996. *Proc. ODP, Sci. Results,* 148: College Station, TX (Ocean Drilling Program).

[2] Ocean Drilling Program, Texas A&M University Research Park, 1000 Discovery Drive, College Station, TX 77845-9547, U.S.A. stokking@cook.tamu.edu

[3] Department of Geology and Geophysics, University of Edinburgh, The Grant Institute, West Mains Road, Edinburgh EH9 3JW, United Kingdom. simona@glg.ed.ac.uk

[4] Bundesanstalt für Geowissenschaften und Rohstoffe, Stilleweg 2, Postfach 510153, D-30631 Hannover, Federal Republic of Germany.

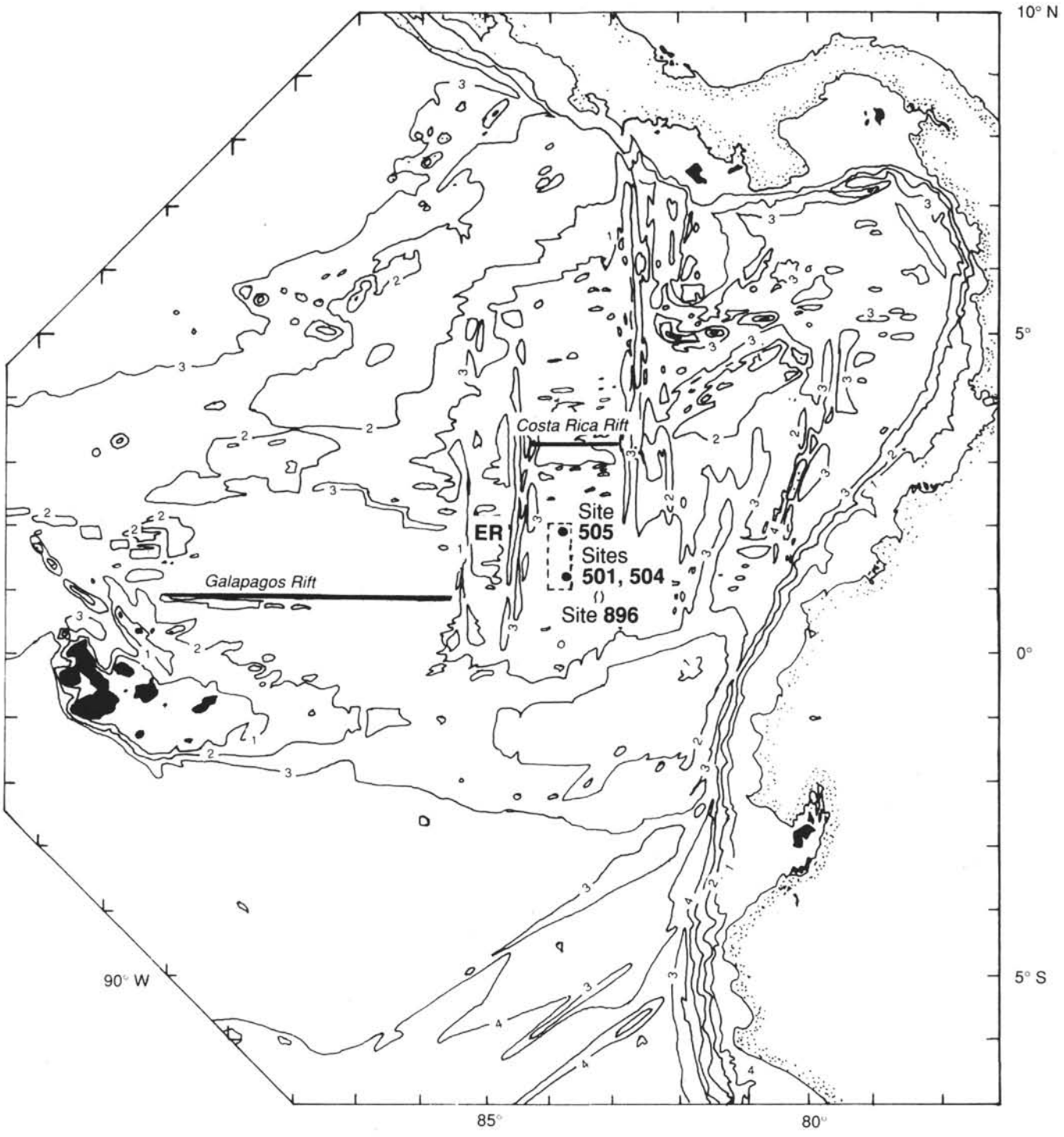

Figure 1. Location of Holes 504B and 896A (after Hobart et al., 1985).

be detected by the disagreement between the bulk composition of a grain (determined by electron microprobe analysis) and the Curie temperature (the temperature above which a mineral behaves paramagnetically and cannot retain a magnetic remanence) predicted on the basis of that bulk composition (Evans and Wayman, 1974; Rice et al., 1980; Smith and Banerjee, 1986; Smith et al., 1991).

Deuteric oxidation of titanomagnetites has been classified by Ade-Hall et al. (1968) and modified by Haggerty (1991). Hall and Fisher (1987) describe stages of hydrothermal alteration of titanomagnetites. According to Ade-Hall et al. (1968) and Haggerty (1991), C1 grains are optically homogeneous titanomagnetite, C2 titanomagnetites contain some exsolved ilmenite lamellae along the (111) plane, C3 grains contain Ti-poor magnetite lamellae intergrown with exsolved ilmenite (up to 50% of grain), and C4 grains display mottling that represents the formation of ferrirutile or exsolved spinel. Hydrothermal alteration stages (Hall and Fisher, 1987) begin with H1, in which there is no evidence of hydrothermal alteration. In H2 grains, fine titanite grains begin to replace ilmenite lamellae. Replacement of ilmenite lamellae by titanite is complete in H3 grains. Progression of alteration in H4 grains is marked by loss of

Fe from magnetite lamellae. Anatase or rutile replaces 50% of H5 grains and 100% of H6 grains (Hall and Fisher, 1987).

In this study, magnetic minerals are identified and characterized on the basis of reflected and transmitted light microscopy in conjunction with electron microprobe analysis, thermal and alternating field demagnetization behavior, anhysteretic and isothermal remanence acquisition, and hysteresis parameters. Alternating field (AF) demagnetization yields the coercivity spectrum (a property that, assuming the sample contains a single type of magnetic carrier, is itself dependent on the grain-volume spectrum in the rock), and indicates whether the coercivity determined by measurement of hysteresis represents that of the carrier of remanence. Measurement of magnetic hysteresis (the magnetization behavior exhibited by a sample in the presence of an increasing magnetic field) will determine coercivity, saturation remanence, and saturation magnetization. These parameters, in conjunction with coercivity of remanence (a measurement of the reverse field required to remove saturation isothermal remanence), will then provide constraints on the domain state of the magnetic minerals in the sample (Dunlop, 1969).

Site 504

The Hole 504B basement section includes 571.5 m of pillow lavas and minor flows, underlain by a 209-m transition zone of mixed pillow lavas, thin flows and dikes, and 1056.0 m of sheeted dikes and massive units (Fig. 2; Alt, Kinoshita, Stokking, et al., 1993). Lithologic units identified during Leg 148 (Alt, Kinoshita, Stokking, et al., 1993) include sparsely to moderately phyric plagioclase-olivine-pyroxene and olivine-plagioclase ± pyroxene diabase. Average silicate grain size ranges from 0.4 to 1.0 mm, whereas that of titanomagnetite ranges from 0.02 to 0.45 mm. Exsolution lamellae of ilmenite are visible in the larger grains, and about half the units contain trace amounts of chrome spinel (Alt, Kinoshita, Stokking, et al., 1993).

Alteration is heterogeneous throughout the interval recovered during Leg 148 (Fig. 2; Alt, Kinoshita, Stokking, et al., 1993). Pervasive background alteration is slight to moderate, whereas more strongly altered regions form centimeter- to decimeter-sized patches and surround veins. Talc + magnetite, chlorite + quartz, actinolite ± magnetite replace interstitial material, and titanite partly replaces igneous magnetite (Alt, Kinoshita, Stokking, et al., 1993).

Magnetic susceptibilities of shipboard samples average 0.018 ± 0.013 SI, similar to values measured from dikes drilled during Legs 111, 137, and 140. The steeply inclined drilling-induced remanence that overprinted shallower dikes was not observed in Leg 148 cores: the bottom-hole assembly used on Leg 148 was new and had therefore never been magnafluxed (Alt, Kinoshita, Stokking, et al., 1993). Thus, natural remanent intensities measured on board ship (mean = 0.48 ± 0.39 A/m) were lower, mean destructive fields were higher, and the properties measured were more representative of in situ values than those determined from dikes recovered during earlier visits to Hole 504B. A relatively weak viscous component was removed by alternating field demagnetization at 20 mT (Alt, Kinoshita, Stokking, et al., 1993).

Site 896

Cores recovered from Hole 896A contained massive basalt, pillow lavas, breccias, and dikes. The basalts are predominantly sparsely to highly phyric plagioclase-olivine basalts or olivine-plagioclase basalts, both commonly containing spinel (Fig. 3; Alt, Kinoshita, Stokking, et al., 1993).

The interval recovered from Hole 896A is divided into two zones on the basis of igneous petrology and magnetic properties. The boundary between the two zones corresponds to the top of a thick sequence of massive units at 390 mbsf. In the upper section, plagioclase is the predominant phenocryst, whereas in the lower section, olivine dominates the phenocryst assemblage. Oxidative alteration, characterized by red alteration halos and by the replacement of olivine with smectite, is most visible in the massive units of the lower section (Alt, Kinoshita, Stokking, et al., 1993).

The intensity of natural remanence is relatively high in the upper part of the hole (shipboard samples: 11.9 A/m), the median destructive field is high (shipboard samples: 22.6 mT), and the bulk susceptibility is relatively low (shipboard samples: 0.015 SI). Stable inclinations measured from samples from the upper part are consistent and average −9.5° ± 10.4° (Allerton et al., this volume; Alt, Kinoshita, Stokking, et al., 1993).

NRM intensity is lower in the lower part of the hole (shipboard samples: 3.9 A/m), median destructive fields are lower (shipboard samples: 12.3 mT), and bulk susceptibilities are higher (shipboard samples: 0.033 SI). Alternating field demagnetization generally isolates two components: a low-coercivity phase, probably carried by titanomagnetite and/or titanomaghemite; and a higher coercivity phase, probably carried by secondary iron oxides and oxyhydroxides (Alt, Kinoshita, Stokking, et al., 1993). Stable inclination data vary widely and are discussed in Allerton et al. (this volume).

METHODS

Hysteresis behavior of 14 samples was measured using a Princeton Applied Research vibrating sample magnetometer in the Paleomagnetic Laboratory in the Geology Department of the University of California, Davis. Sample sizes in this study ranged from 0.005 to 0.0098 mg. Hysteresis measurements are made by applying an increasing magnetic field to a sample, then reversing the applied field, while continually measuring the magnetization of the sample as it responds to the changing applied field. A plot of applied field vs. sample magnetization results in a loop, the shape of which is determined by the chemical composition, microstructure, and particle orientation of the magnetic material within the sample (Stacey and Banerjee, 1974; Day et al., 1977; Cisowski, 1980). The hysteresis parameters saturation remanence (J_{RS}), saturation magnetization (J_S), and coercivity (H_C) are obtained from the hysteresis loop. Coercivity of remanence (H_{CR}) was determined using the vibrating sample magnetometer on the samples whose hysteresis behavior was studied. A field of 1.2 T was used to saturate the samples.

Before proceeding with alternating-field (AF) demagnetization, intensities of natural remanent magnetization (NRM) of 19 samples from Hole 504B and 71 samples from Hole 896A were measured on board the *JOIDES Resolution* (Alt, Kinoshita, Stokking, et al., 1993). NRM intensities of 15 additional samples from Hole 504B and of 41 additional samples from Hole 896A were measured in the Paleomagnetic Laboratory at Texas A&M University (TAMU). On the *Resolution,* both a Molspin spinner magnetometer and a 2-G Enterprises (Model 760R) pass-through cryogenic rock magnetometer were used. At TAMU, NRM intensities were measured on a three-axis CTF cryogenic magnetometer housed in a shielded room at TAMU, and corrected by sample volume. Magnetic susceptibilities of discrete samples on board ship were determined using a Kappabridge KLY-2. Magnetic susceptibilities of samples in this study were measured at TAMU using a Bartington Instruments Susceptibility Meter at a frequency of 0.47 kHz, and corrected by sample volume. Three samples from Hole 896A were thermally demagnetized using a Schonstedt thermal demagnetizer (Model TSD-1) at TAMU. Samples were heated at temperature intervals between 20°C and 50°C up to 600°C and the remanence measured between steps.

Studies of acquisition of isothermal remanent magnetization (IRM) and anhysteretic remanent magnetization (ARM) were performed on board ship during Leg 148 (Alt, Kinoshita, Stokking, et al., 1993). Shipboard ARMs were produced using alternating fields up to 100 mT and a DC-biased field of 0.032 mT (Alt, Kinoshita, Stokking, et al., 1993). Few samples, however, were fully saturated by the maximum applied field.

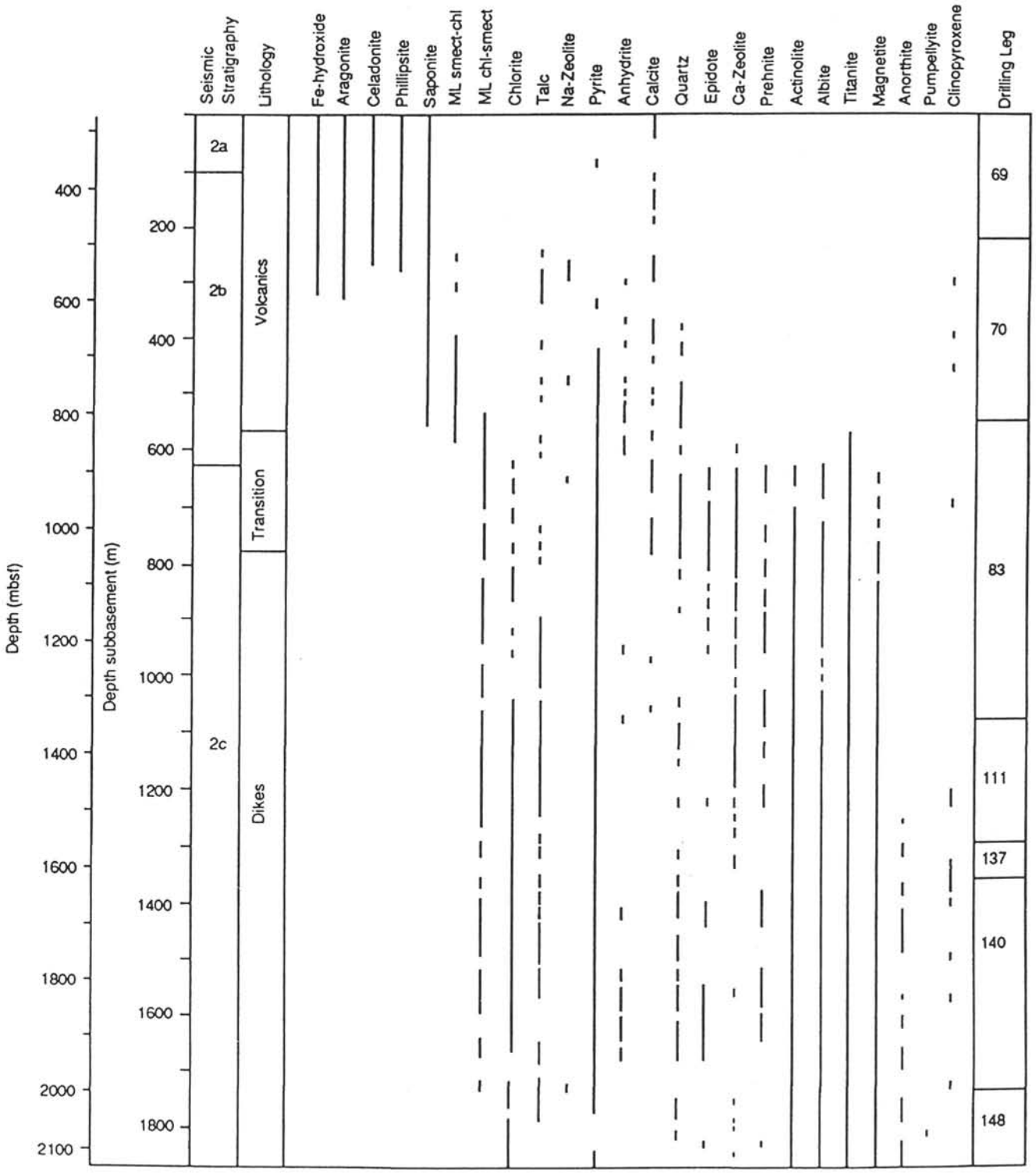

Figure 2. Distribution of secondary mineralogy, seismic stratigraphy, and lithology in Hole 504B (from Alt et al., 1986; Becker, Sakai, et al., 1989; Alt, Kinoshita, Stokking, et al., 1993).

On board ship, an AF demagnetizer (Model 2G600) capable of producing an alternating field up to 20 mT was used on-line with the pass-through cryogenic magnetometer. AF demagnetization at higher fields was performed using a single-axis Schonstedt Geophysical Specimen Demagnetizer (Model GSD-1) capable of producing alternating fields up to 100 mT. At TAMU, samples were AF demagnetized using Schonstedt Geophysical Specimen Demagnetizer (Model GSD-1). Samples were analyzed using the cryogenic magnetometers between AF steps.

After AF demagnetization at TAMU, a maximum ARM was subsequently imparted to 52 samples using an alternating field of 100 mT and a DC bias field of 0.05 mT. The Schonstedt AF demagnetizer

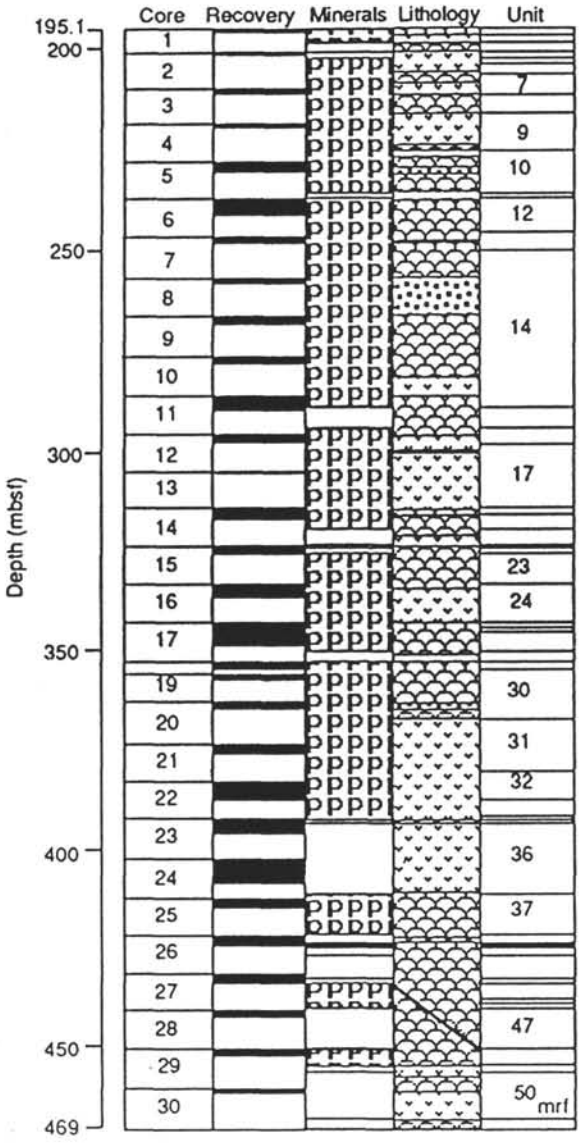

Figure 3. Drilling and recovery at Hole 896A. Black bars show recovery relative to core length. The dominant phenocryst is olivine, except where the symbol "P" in the minerals column is employed to indicate that plagioclase is dominant. Symbols in the lithology column indicate eruptive type: pillow basalts = convex upward, massive = "V", and breccia = solid. A mixture of pillow basalts, pillow-breccias, and breccias is indicated by a solid diagonal line (Alt, Kinoshita, Stokking, et al., 1993).

and an anhysteretic magnetizer constructed at TAMU by W. Sager were used to produce the ARM. The ARM of 16 samples was then AF demagnetized so the demagnetization behavior could be compared with that of NRM and IRM.

An IRM was applied at a maximum field of 1.0 T to 53 samples in the study using an ASC, Inc., impulse magnetizer (Model IM-10) and measured using the CTF cryogenic magnetometer. Sixteen pilot samples were given an IRM at 1.0 T and AF demagnetized so the demagnetization of IRM could be compared with that of NRM and ARM.

After all magnetic analyses were performed, polished thin sections were made from 10 representative samples. The thin sections were studied using reflected light microscopy and representative sections were selected from electron microanalysis. Electron microprobe analyses were performed to determine the chemical composition (major and trace elements) of the opaque minerals. Ulvöspinel content (X) was calculated as follows:

$$X = 3/(1 + \mathrm{Fe/Ti}),$$

where $\mathrm{Fe/Ti} = (0.777\mathrm{FeO} + 0.696\mathrm{Fe_2O_3})/(0.6\mathrm{TiO_2})$.

Opaque minerals were analyzed with a Cameca SX-50 automated electron microprobe in the TAMU Geology Department, using a finely focused (≈1 μm), nonrastered, spot-fixed electron beam. During analysis, the beam current was 30 nA at 15 kev for thin sections from Hole 504B and 10 nA at 15 kev for thin sections from Hole 896A, which contained larger oxide grains. For ilmenite, magnetite, and maghemite analyses, Si and Ca were each counted for 10 s; Ti and Fe were each counted for 20 s; V, Ni, and Zn were each counted for 30 s; Mn and Cr were each counted for 40 s; Mg was counted for 100 s; and Al was counted for 110 s. For the titanite analyses, Ca and Ti were each counted for 20 s, Mn and Fe were each counted for 60 s, and Mg and Si were each counted for 80 s. Natural mineral standards used were diopside, spinel, $FeTiO_3$, chromite, ilmenite, spessartine, and gahnite. Metal standards used were nickel and vanadium. Titanomagnetite and titanomaghemite weight percentages were recalculated following the method of Carmichael (1967) on the basis of 4 oxygens using a BASIC program obtained from J. Allan. Fe^{3+} values were determined by charge balance. Calculations for ilmenite and titanite followed the Cameca program, which uses the Deer et al. (1962) formulas. Ilmenite analyses were normalized by 6 oxygens, and titanite analyses were normalized by 18 oxygens.

RESULTS

Rock Magnetic Properties

Table 1 summarizes the hysteresis parameters of the samples studied. In this sample set, coercivity of Hole 504B samples ranges from 0.9 to 13.7 mT (mean = 5.46 mT), coercivity of remanence ranges from 12.5 to 38.6 mT (mean = 23.0 mT), the ratio H_{CR}/H_C ranges from 2.8 to 15.70 mT (mean = 8.31). Saturation magnetization (J_S) ranges from 1.17 to 66.2 mAm^2/kg (mean = 28.09 mAm^2/kg), saturation remanence (J_{RS}) ranges from 0.016 to 2.57 mAm^2/kg (mean = 0.77 mAm^2/kg), and the ratio J_{RS}/J_S ranges from 0.012 to 0.154 (mean = 0.06). Coercivity of Hole 896A samples ranges from 0.04 to 9.07 mT (mean = 3.33 mT), coercivity of remanence ranges from 7.24 to 26.8 mT (mean = 13.6 mT), the ratio H_{CR}/H_C ranges from 2.05 to 181 mT (mean = 32.2). Saturation magnetization (J_S) ranges from 2.34 to 46.9 mAm^2/kg (mean = 13.9 mAm^2/kg), saturation remanence (J_{RS}) ranges from 0.012 to 9.2 mAm^2/kg (mean = 1.39 mAm^2/kg), and the ratio J_{RS}/J_S ranges from 0.012 to 0.154 (mean = 0.076).

Additional rock magnetic data from Hole 504B samples in the study are presented in Table 2. NRM intensity ranges from 0.01 to 0.24 A/m (mean = 0.09 A/m). IRM intensity acquired at 1.0 T ranges from 6.79 to 445.89 A/m (mean = 155.9 A/m) and saturation ARM (SARM) ranges from 0.05 to 0.80 A/m (mean = 0.37 A/m). Data from Hole 896A samples are presented in Table 3. NRM intensity ranges from 0.14 to 22.59 A/m (mean = 5.06 A/m). Saturation IRM ranges from 95.59 to 451.95 A/m (mean = 261.77 A/m) and saturation ARM ranges from 0.47 to 7.31 A/m (mean = 3.69 A/m).

Figure 4 illustrates representative AF demagnetization behavior of NRM, IRM, and ARM for Samples 148-504B-247R-1, 60–62 cm, and 252R-1, 33–35 cm, and for Samples 148-896A-8R-1, 74–76 cm, and 24R-4, 84–86 cm. Sample 148-504B-247R-1, 60–62 cm, is a sparsely phyric plagioclase-olivine diabase containing about 10% patchy groundmass alteration. Sample 148-504B-252R-1, 33–35 cm, is a moderately phyric plagioclase-olivine-clinopyroxene diabase. Samples 148-896A-8R-1, 74–76 cm, and 24R-4, 84–86 cm, are moderately phyric plagioclase-olivine basalt. In these, as in all samples

Table 1. Hysteresis data from Holes 504B and 896A.

Core, section, interval (cm)	Depth (mbsf)	Unit	Lith	H_C (mT)	H_{CR} (mT)	H_{CR}/H_C	J_S (mAm^2/kg)	J_{RS} (mAm^2/kg)	J_{RS}/J_S
148-504B-									
241R-1, 115–117	2017.65	276	POC	5.10	23.80	4.67	47.37	2.57	0.05
247R-1, 14–18	2056.84	285	PO	0.90	12.50	13.89	40.10	0.02	0.01
247R-1, 60–62	2057.30	285	PO	1.60	15.40	9.63	66.20	0.51	0.02
249R-1, 81–84	2072.01	290	CP	0.93	14.60	15.70	8.39	0.10	0.01
251R-1, 17–22	2090.07	293	POC	10.50	32.90	3.13	5.31	1.25	0.11
252R-1, 33–37	2099.73	293	POC	13.70	38.60	2.82	1.17	0.18	0.15
Max				13.70	38.60	15.70	66.20	2.57	0.15
Min				0.90	12.50	2.82	1.17	0.02	0.01
Mean				5.46	22.97	8.31	28.09	0.77	0.06
SD				5.47	10.78	5.62	26.83	0.99	0.06
148-896A-									
8R-1, 74–76	257.84	14	PO	8.15	16.70	2.05	46.90	9.20	0.20
11R-1, 91–93	286.91	14	PO	6.01	17.20	2.86	5.84	0.71	0.12
16R-2, 81–83	336.06	24	OP	0.04	7.24	181.00	9.13	0.01	0.00
16R-2, 117–120	336.42	24	OP	0.43	9.82	22.84	13.30	0.01	0.01
21R-3, 29–31	376.27	32	PO	9.07	26.80	2.95	2.34	0.46	0.20
22R-2, 64–66	384.73	32	PO	1.91	13.10	6.86	6.68	0.37	0.06
24R-4, 84–86	407.08	36	PO	0.29	7.39	25.40	15.30	0.11	0.01
30R-1, 134–136	460.64	51	OP	0.77	10.60	13.73	11.70	0.22	0.02
Max				9.07	26.80	181.00	46.90	9.20	0.20
Min				0.04	7.24	2.05	2.34	0.01	0.00
Mean				3.33	13.61	32.21	13.90	1.39	0.08
SD				3.79	6.54	60.81	13.99	3.17	0.08

Notes: Max = maximum, Min = minimum, Lith = lithology, POC = plagioclase-olivine-clinopyroxene diabase, CP = clinopyroxene-plagioclase phyric diabase, PO = plagioclase-olivine diabase, and OP = olivine-plagioclase diabase. Other abbreviations defined in the text.

for which demagnetization of NRM, ARM, and IRM were compared, ARM is more stable to AF demagnetization than is IRM. Median destructive field (MDF) values for NRMs from Hole 504B range from 7 to 60 mT, with a mean of 31 mT. Hole 896A samples had MDFs ranging from 5 to 50 mT and averaged 16 mT. Thermally demagnetized samples from Hole 896A showed inversion to hematite at about 300°C, characteristic of titanomaghemite.

Volume susceptibility from Hole 504B samples ranges from 0.0014 to 0.098 (mean = 0.032 ± 0.029 SI) similar to the mean value of the dikes obtained during previous legs (0.016–0.018 SI units; Pariso and Johnson, 1991; Pariso et al., 1995). Volume susceptibility from Hole 896A samples ranges from 0.002 to 0.104 SI (mean = 0.027 ± 0.025 SI).

Magnetic Oxide Petrography and Chemistry

Three samples from Hole 504B were analyzed using the electron microprobe. Major- and trace-element geochemical analyses are presented in Tables 4, 5, and 6. Letters appended to sample names in the tables refer to different grains within the same thin section. A backscattered electron image from Sample 148-504B-247R-1, 60–62 cm, is presented in Figure 5.

Seven samples from Hole 896A were studied by electron microanalysis. Major- and trace-element geochemical analyses are presented in Table 7. Letters appended to sample names in the tables refer to different grains within the same thin section. Figures 6A–E are backscattered electron images of representative samples from Hole 896A that illustrate the range of grain morphologies observed.

DISCUSSION AND CONCLUSIONS

Hole 504B

NRM and Susceptibility

The range of NRM intensities measured in this suite of samples is consistent with that reported in Pariso et al. (1995), which reflects a general slight increase with depth in the sheeted dike section. Shipboard measurements during Leg 148 and the results presented here

Table 2. Rock-magnetic data for Hole 504B samples.

Core, section, interval (cm)	Depth (mbsf)	Unit	Lith	NRM (A/m)	MDF	IRM (A/m)	SARM (A/m)	K (SI)
148-504B-								
240R-1, 15–26	2007.05	272	P	0.01	12	223.54	0.57	0.0181
241R-1, 27–29	2016.77	276	POC	0.04	35	445.89	0.20	0.0215
241R-1, 115–117*	2017.65	276	POC	0.03	42	30.85	0.12	0.0041
246R-1, 70–73*	2052.90	283	P	0.24	7	132.67	0.57	0.0538
247R-1, 14–18*	2056.84	285	PO	0.06	37	81.18	0.45	0.0819
247R-1, 60–62*	2057.30	285	PO	0.17	12	317.21	0.80	0.0980
249R1, 8–11	2071.28	289	A	0.24	15	165.46	0.43	0.0308
249R-1, 81–84	2072.01	290	PO	0.08	25	122.24	0.27	0.0333
250R-1, 105–109	2081.45	292	POC	0.11	25	306.25	0.62	0.0179
251R-1, 17–22*	2090.07	293	POC	0.04	45	11.12	0.13	0.0031
251R-1, 25–27	2090.15	293	POC	0.09	40	160.38	0.43	0.0315
251R-1, 39–41	2090.29	293	POC	0.19	25	190.13	0.58	0.0491
251R-1, 80–85	2090.70	293	POC	0.04	60	133.11	0.28	0.0273
252R-1, 11–15	2099.51	293	POC	0.03	45	11.69	0.10	0.0016
252R-1, 33–37*	2099.73	293	POC	0.02	45	6.79	0.05	0.0014
Max				0.24	60	445.89	0.80	0.0980
Min				0.01	7	6.79	0.05	0.0014
Mean				0.09	31	155.90	0.37	0.0316
SD				0.08	15	127.05	0.23	0.0288

Notes: Max = maximum, Min = minimum, SD = standard deviation, Lith. = lithology, P = plagioclase phyric diabase, POC = plagioclase-olivine-clinopyroxene diabase, PO = plagioclase-olivine diabase, and A = aphyric diabase. K = volume susceptibility. Asterisks indicate samples with NRM, ARM, and IRM values that were AF demagnetized and compared. Other abbreviations defined in the text.

are lower than those reported from earlier legs to Site 504: the mean shipboard NRM from Leg 148 samples was 0.48 A/m (Alt, Kinoshita, Stokking, et al., 1993) and that of samples in this study is 0.09 A/m. Leg 137/140 shipboard measurements averaged 3.0 A/m (Dick, Erzinger, Stokking, et al., 1993). The Leg 148 MDF averaged 25 mT (Alt, Kinoshita, Stokking, et al., 1993), average MDF for samples in this study is 31, and that of Leg 137/140 samples was only 9.6 mT (Dick, Erzinger, Stokking, et al., 1992). Leg 148 shipboard paleomagnetists attributed these variations to the presence of a drilling-induced remanence, which affected the Leg 137/140 samples but not the Leg 148 material because of differences between the bottom-hole drilling assemblies used for Legs 137/140 and 148, rather than to differences in in-situ rock magnetic properties. Leg 148 samples are thus more representative of the actual in-situ values than are Leg 137/

Table 3. Rock-magnetic data for Hole 896A samples.

Core, section, interval (cm)	Depth (mbsf)	Unit	Lith	Structure	% Ox	NRM (A/m)	MDF (mT)	K (SI)	SARM (A/m)	IRM (A/m)
148-896A-										
2R-1, 5–12	200.95	4	OP	Massive	100	5.86	20	0.0067	3.26	253.53
2R-1, 32–38	201.22	5	OP	Massive	100	9.25	40	0.0124	6.08	246.39
4R-1, 106–112	219.96	10	PO	Pillow	100	4.33	TH	0.0192		
8R-1, 74–76*	257.84	14	PO	Pillow	95	11.52	20	0.0020		288.02
10R-1, 111–113	277.51	14	PO	Pillow	35	22.59		0.0036	6.27	332.95
11R-1, 15–17	286.15	14	PO	Pillow	70	10.34	27	0.0160	5.35	372.40
11R-1, 91–93	286.91	14	PO	Pillow	0	13.80		0.0054	3.28	279.76
12R-2, 19–22	297.24	16	OP	Pillow/massive	50	7.35	45	0.0076	0.47	317.68
14R-3, 61–63	318.09	21	OP	Pillow/massive	100	8.55	15	0.0179	3.97	231.97
15R-2, 19–21	325.88	23	OP	Pillow	0	11.50	32	0.0142	5.22	339.12
16R-1, 118–120	335.08	24	OP	Massive	35	5.82	10	0.0420	3.12	256.88
16R-2, 81–83*	336.06	24	OP	Massive	60	4.68	10	0.0351	3.74	294.85
16R-2, 117–120*	336.42	24	OP	Massive	15	7.25	5	0.0285	3.78	270.56
16R-3, 51–53*	337.21	24	OP	Massive	60	4.56	5	0.0288	3.86	268.92
16R-3, 122–124	337.92	24	OP	Pillow	0	15.26	17	0.0165	6.37	374.58
17R-3, 26–28	346.7	27	OP	Pillow	50	3.91	15	0.0233	2.55	255.82
20R-1, 118–120	364.08	31	PO	Massive	90	2.45	12	0.0203	4.72	344.58
20R-1, 142–144	364.92	31	PO	Massive	95	2.94	12	0.0143	4.13	325.09
21R-3, 29–31*	376.27	32	PO	Massive	0	8.76	27	0.0129	7.31	451.95
22R-1, 0–5	382.6	32	PO	Massive	10	7.10	17	0.0184	5.88	404.48
22R-2, 64–66*	384.73	32	PO	Massive	50	2.33	15	0.0157	4.57	337.07
22R-3, 129–131	386.88	33	PO	Massive	60	9.91	10	0.0219	5.10	403.69
23R-3, 42–44	395.42	36	PO	Massive	100	0.39	5	0.0335	1.48	110.35
24R-1, 8–10	401.88	36	PO	Massive	7	2.59	TH	0.0718		
24R-1, 111–113	402.91	36	PO	Massive	0	0.68	5	0.0271	2.18	95.59
24R-2, 15–17	403.45	36	PO	Massive	85	1.06	5	0.0108	2.32	194.29
24R-3, 32–35	405.1	36	PO	Massive	90	1.61	TH	0.0585		
24R-3, 94–96*	405.72	36	PO	Massive	100	1.58	5	0.1037	2.32	140.22
24R-4, 63–65	406.87	36	PO	Massive	75	1.53	5	0.0687	2.80	212.07
24R-4, 84–86*	407.08	36	PO	Massive	80	0.67	5	0.0115	3.25	163.00
24R-5, 45–47	408.13	36	PO	Massive	85	1.28	7	0.0134	2.82	258.72
24R-5, 77–79	408.45	36	PO	Massive	100	2.94	7	0.0902	3.06	261.28
24R-5, 125–127	408.93	36	PO	Massive	98	3.24	7	0.0094	2.30	188.18
25R-1, 124–126	412.54	37	PO	Pillow	60	1.64	20	0.0095	2.65	231.02
26R-1, 74–76	421.74	38	OP	Massive	98	2.56	12	0.0075	3.59	270.79
27R-1, 41–44	430.91	42	OP	Breccia	5	0.47	35	0.0117	4.00	118.16
27R-1, 52–54	431.02	42	OP	Massive	0	1.55	50	0.0130	3.70	224.19
27R-1, 55–57	431.05	42	OP	Breccia	0	0.14	25	0.0195	2.45	146.21
27R-3, 29–31	433.66	46	PO	Pillow	5	2.08	15	0.0501	3.53	220.18
29R-1, 115–117*	450.85	49	OP	Massive	85	0.90	5	0.0274	2.36	175.14
30R-1, 134–136*	460.64	51	OP	Pillow	10	0.69	10	0.0934	2.86	287.60
Max						22.59	50	0.1037	7.31	451.95
Min						0.14	5	0.0020	0.47	95.59
Mean						5.06	16	0.0272	3.69	261.77
SD						4.91	12	0.0254	1.48	85.37

Notes: Max = maximum, Min = minimum, SD = standard deviation, Lith = lithology, OP = olivine-plagioclase phyric basalt, PO = plagioclase-olivine phyric basalt, % Ox = percentage of groundmass alteration (from "Alteration Log" in Alt, Kinoshita, Stokking, et al., 1993). *K* = volume susceptibility. Asterisks indicate samples whose NRM, ARM, and IRM were AF demagnetized and compared. Other abbreviations defined in the text.

140 samples (Alt, Kinoshita, Stokking, et al., 1993). Differences between the average value of shipboard data and data presented in this study may reflect the smaller number of samples in this study and/or correction of remanence data in this study by actual (rather than assumed) sample volume.

Magnetic remanence (natural and laboratory-induced) and magnetic susceptibility reflect the concentration of magnetic carriers in the rock. Samples whose magnetic intensity is low also have low magnetic susceptibility (Table 2) and low saturation magnetization (Table 1), as discussed in Pariso et al. (1995) and implying that the low remanence and susceptibility values reflect a decrease in the amount of magnetite. This variation in concentration of magnetite in turn reflects hydrothermal alteration, which causes loss of iron and replacement of ilmenite by anatase and/or rutile (Pariso and Johnson, 1991; Pariso et al., 1995). As observed by Pariso and Johnson (1991) and Pariso et al. (1995), samples whose magnetic intensity and susceptibility are low show evidence of high degrees of hydrothermal alteration, whereas samples whose magnetic intensity and susceptibility are moderate to high are less altered. Thus, variability in the amount of magnetizable material produced by differing degrees of hydrothermal alteration of the samples results in the wide variation in rock magnetic properties observed in this suite of samples.

IRM and ARM

Studies of acquisition of isothermal remanent magnetization (IRM) and anhysteretic remanent magnetization (ARM) were performed on board ship during Leg 148 (Alt, Kinoshita, Stokking, et al., 1993). Shipboard samples saturated in applied fields ranging from 90 and 200 mT, consistent with magnetite and/or titanomagnetite as the predominant remanence carrier, with a minor amount of higher coercivity minerals, such as hematite (Alt, Kinoshita, Stokking, et al., 1993). Shipboard ARMs were acquired in alternating fields up to 100 mT, and in DC-biased fields of 0.032 mT, similar to that prevailing at Earth's field at Site 504 (Alt, Kinoshita, Stokking, et al., 1993). The shapes of ARM and IRM acquisition curves are consistent with the predominant magnetic carrier in Hole 504B being low-titanium magnetite.

Magnetic Oxide Petrography and Chemistry

The predominant magnetic oxide mineral in Hole 504B rocks recovered during Leg 148 is low-titanium magnetite, produced during high-temperature (greater than 500°– 600°C) deuteric oxidation of primary titanomagnetite to magnetite plus ilmenite (Pariso and

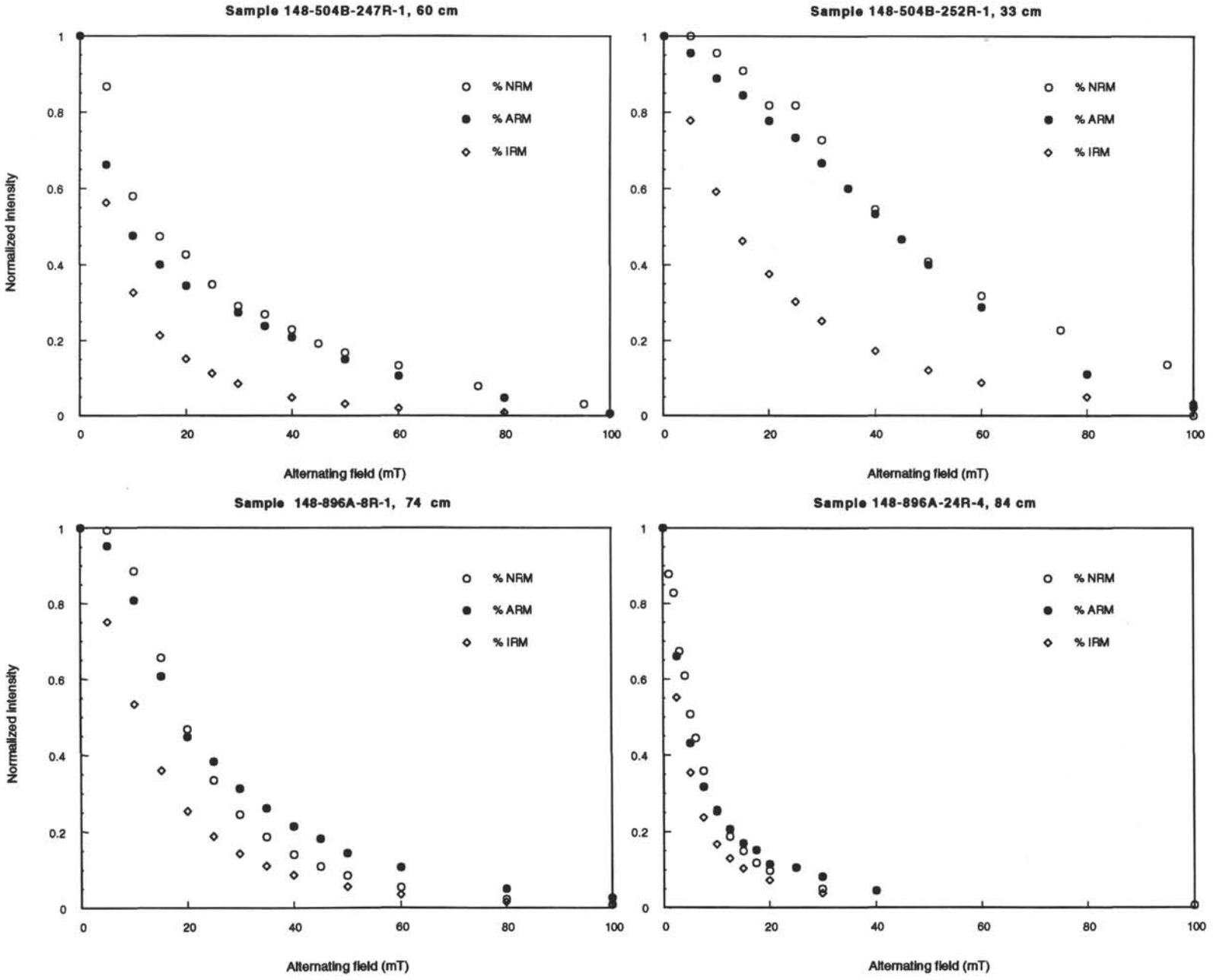

Figure 4. Alternating field (AF) demagnetization of NRM (open circles), ARM (filled circles), and IRM (diamonds) from representative samples.

Table 4. Major- and trace-element analyses of magnetite lamellae from Hole 504B samples.

Core, section, interval (cm)	SiO_2	TiO_2	Al_2O_3	V_2O_3	Cr_2O_3	MnO	NiO	ZnO	MgO	CaO	FeO	Fe_2O_3	Total	Fe/Ti	*X*
148-504B-															
246R-1, 70–73a	0.055	0.683	0.019	0.706	0.089	0.029	0.048	0.051	0.003	0.301	31.612	67.502	101.098	174.582	0.017
246R-1, 70–73b	0.111	1.145	0.040	0.464	0.049	0.029	0.000	0.017	0.031	0.171	32.301	66.727	101.085	104.134	0.029
246R-1, 70–73c	0.133	2.114	0.729	0.712	0.069	0.082	0.002	0.000	0.005	0.115	33.292	63.403	100.656	55.185	0.053
246R-1, 70–73c	0.095	2.325	0.337	0.759	0.083	0.091	0.021	0.163	0.008	0.035	33.534	64.014	101.465	50.616	0.058
247R-1, 60–62a	0.083	1.950	1.134	1.221	0.135	0.037	0.031	0.094	0.004	0.072	33.423	63.389	101.573	59.905	0.049
247R-1, 60–62a	0.201	2.226	0.192	0.887	0.066	0.047	0.048	0.047	0.023	0.071	33.612	64.020	101.440	52.916	0.056
247R-1, 60–62b	0.115	1.808	1.237	0.792	0.066	0.074	0.000	0.000	0.008	0.092	33.068	63.269	100.529	64.278	0.046
247R-1, 60–62b	0.083	1.514	0.913	0.852	0.088	0.044	0.017	0.000	0.014	0.021	32.903	64.459	100.908	77.531	0.038
247R-1, 60–62c	0.091	2.252	0.489	0.423	0.040	0.112	0.000	0.012	0.003	0.088	32.968	63.072	99.550	51.446	0.057
Max	0.201	2.325	1.237	1.221	0.135	0.112	0.048	0.163	0.031	0.301	33.612	67.502	101.573	174.582	0.058
Min	0.055	0.683	0.019	0.423	0.040	0.029	0.000	0.000	0.003	0.021	31.612	63.072	99.550	50.616	0.017
Mean	0.107	1.780	0.566	0.757	0.076	0.061	0.019	0.043	0.011	0.107	32.968	64.428	100.923	76.733	0.045
SD	0.042	0.563	0.460	0.236	0.028	0.030	0.020	0.055	0.010	0.085	0.647	1.596	0.628	40.493	0.014

Notes: Max = maximum, Min = minimum, and SD = standard deviation. Value *X* (ulvöspinel content) explained in text. Lowercase letters appended to centimeter intervals refer to different grains within the same thin section.

Table 5. Major- and trace-element analyses of ilmenite lamellae from Hole 504B samples.

Core, section, interval (cm)	V_2O_5	SiO_2	TiO_2	Al_2O_3	Cr_2O_3	Fe_2O_3	MgO	CaO	MnO	FeO	NiO	ZnO	Total	Fe/Ti
148-504B-														
246R-1, 70–73a	0.5555	0.0443	44.5170	0.0337	0.0319	13.8480	0.0080	0.2809	1.3272	38.7112	0.0162	0.0000	99.3739	1.4870
246R-1, 70–73b	0.4127	0.0142	46.2403	0.0117	0.0129	11.8759	0.0365	0.2292	1.8072	39.6993	0.0046	0.0175	100.3619	1.4097
246R-1, 70–73b	0.4701	2.6309	45.6242	0.0874	0.0239	8.9141	0.0878	1.1944	1.6197	39.3021	0.0000	0.0000	99.9546	1.3422
246R-1, 70–73c	0.4727	0.0675	47.4400	0.0044	0.0357	9.7348	0.0276	0.2599	1.7500	40.8574	0.0000	0.0512	100.7012	1.3533
246R-1, 70–73c	0.4995	0.0046	47.0008	0.0049	0.0186	9.8896	0.0306	0.2852	1.7672	40.4320	0.0039	0.0000	99.9367	1.3581
247R-1, 60–62a	0.7132	0.0726	47.2611	0.3818	0.0381	9.2879	0.1170	0.0198	1.9069	40.6454	0.0362	0.0100	100.4900	1.3417
247R-1, 60–62a	0.8977	0.1750	47.8786	0.2739	0.0398	7.6430	0.0943	0.0533	2.2703	40.7978	0.0355	0.0100	100.1691	1.2887
247R-1, 60–62b	0.4021	0.8306	45.0026	0.1421	0.0241	12.0883	0.1225	0.7190	2.0756	38.2583	0.0000	0.0000	99.6652	1.4125
247R-1, 60–62b	0.6195	0.0895	47.1153	0.3555	0.0604	9.5331	0.1306	0.0097	1.9989	40.3889	0.0000	0.0088	100.3100	1.3448
247R-1, 60–62c	0.4650	0.0501	47.5357	0.0405	0.0154	7.4159	0.0744	0.1843	1.9019	40.7221	0.0000	0.0364	98.4417	1.2903
252R-1, 33–37a	0.3103	0.0667	47.0616	0.0103	0.0285	8.4845	0.0781	0.4969	2.0994	40.0741	0.0720	0.0000	98.7823	1.3119
252R-1, 33–37a	0.3359	0.0670	49.5790	0.0051	0.0061	4.7270	0.0775	0.4300	1.9821	42.4435	0.0560	0.0838	99.7930	1.2192
252R-1, 33–37a	0.2965	0.1306	47.2409	0.0308	0.0046	8.2555	0.0969	0.5622	1.9826	40.3232	0.0546	0.0200	98.9985	1.3081
252R-1, 33–37b	0.3224	0.0245	47.4451	0.0093	0.0000	8.6131	0.0484	0.3535	2.6089	39.9417	0.0068	0.0300	99.4038	1.3008
252R-1, 33–37b	0.3055	0.0358	47.1006	0.0089	0.0100	8.7942	0.0391	0.4259	2.2703	39.9957	0.0227	0.0488	99.0576	1.3162
252R-1, 33–37b	0.2790	0.0707	47.3762	0.0128	0.0107	8.2104	0.0426	0.3813	2.4169	40.0919	0.0000	0.0063	98.8989	1.2969
252R-1, 33–37c	0.3929	0.3509	47.8589	0.0901	0.0235	8.0119	0.1370	0.4437	2.1547	40.6839	0.0417	0.0000	100.1891	1.2950
252R-1, 33–37c	0.4580	0.1589	48.4793	0.0382	0.0370	6.5244	0.0717	0.5532	1.9968	41.4879	0.0492	0.0038	99.8585	1.2644
Max	0.8977	2.6309	49.5790	0.3818	0.0604	13.8480	0.1370	1.1944	2.6089	42.4435	0.0720	0.0838	100.7012	1.4870
Min	0.2790	0.0046	44.5170	0.0044	0.0000	4.7270	0.0080	0.0097	1.3272	38.2583	0.0000	0.0000	98.4417	1.2192
Mean	0.4560	0.2714	47.0976	0.0856	0.0234	8.9918	0.0734	0.3824	1.9965	40.2698	0.0222	0.0181	99.6881	1.3300
SD	0.1612	0.6193	1.18262	0.1229	0.0154	2.091522	0.03849	0.2799	0.2971	0.95126	0.0243	0.02347	0.651486	0.0612

Notes: Max = maximum, Min = minimum, and SD = standard deviation. Lowercase letters appended to centimeter intervals refer to different grains within the same thin section.

Table 6. Major- and trace-element analyses of titanite from Hole 504B samples.

Core, section, interval (cm)	SiO_2	MgO	CaO	MnO	TiO_2	FeO	Total
148-504B-							
246R-1, 70–73a	38.114	4.527	21.565	0.087	23.383	6.321	93.997
252R-1, 33–37a	30.396	0.211	28.125	0.041	32.608	2.056	93.437
252R-1, 33–37a	30.462	0.130	28.274	0.029	34.618	1.167	94.680
252R-1, 33–37a	31.410	0.577	27.424	0.039	32.688	1.439	93.577
252R-1, 33–37b	31.029	0.504	27.486	0.000	29.278	1.888	90.185
252R-1, 33–37b	26.556	0.048	22.971	0.043	45.375	1.795	96.788
252R-1, 33–37c	30.273	0.012	28.075	0.048	36.608	1.136	96.152
252R-1, 33–37c	30.594	0.040	28.416	0.008	33.901	1.355	94.314
252R-1, 33–37c	30.420	0.009	28.627	0.008	34.754	0.972	94.790
252R-1, 33–37c	30.578	0.032	28.389	0.041	36.507	0.963	96.510
252R-1, 33–37c	30.128	0.036	28.170	0.064	36.596	1.094	96.088
Max	38.114	4.527	28.627	0.087	45.375	6.321	96.788
Min	26.556	0.009	21.565	0.000	23.383	0.963	90.185
Mean	30.905	0.557	27.047	0.037	34.211	1.835	94.593
SD	2.703	1.332	2.412	0.026	5.370	1.535	1.882

Note: Max = maximum, Min = minimum, and SD = standard deviation. Lowercase letters appended to centimeter intervals refer to different grains within the same thin section.

Johnson, 1991; Pariso et al., 1995). Subsequently, Leg 148 rocks were hydrothermally altered to varying extent: some or all ilmenite lamellae were replaced by titanite and/or a high-titanium mineral (anatase or rutile) and some iron was lost.

In all Hole 504B samples examined, high-temperature oxidation of primary titanomagnetite has produced lamellae or pods of magnetite and ilmenite. Hydrothermal alteration has further altered the minerals to a mixture of magnetite, ilmenite, titanite, and a high-titanium mineral (either rutile or anatase), as discussed in Pariso et al. (1995). Sample 148-504B-246R-1, 70–73 cm, is a sparsely phyric plagioclase-olivine diabase. Hydrothermal alteration of magneto-ilmenite intergrowths falls in classes H1 and H2, and oxidation stage is C3. Intergrowths grains range up to 50 μm in diameter. Sample 148-504B-247R-1, 60–62 cm, is a moderately phyric plagioclase-olivine diabase exhibiting H3 hydrothermal alteration and C2–C3 oxidation. Intergrowths are up to 80 μm in diameter. Sample 148-504B-252R-1, 33–37 cm, is a moderately phyric plagioclase-olivine-clinopyroxene diabase exhibiting H4 to H5 hydrothermal alteration and C4 oxidation.

Table 4 shows that magnetite lamellae tend to be enriched in trivalent elements: Cr_2O_3 averages 0.076 wt% in magnetite relative to 0.023 wt% in ilmenite, Al_2O_3 averages 0.566 wt% in magnetite and

only 0.086 wt% in ilmenite, and V_2O_3 averages 0.757 wt% in magnetite whereas V_2O_5 averages 0.456 wt% in ilmenite. Divalent elements are partitioned into ilmenite lamellae: MnO averages 2.0 wt% in ilmenite and 0.0631 wt% in magnetite, and MgO averages 0.073 wt% in ilmenite and only 0.011 wt% in magnetite. These trends are consistent with those reported for sheeted dike samples from Legs 137 and 140 (Stokking et al., 1995).

Deer et al. (1962) and Haggerty (1976) report the partitioning of divalent ions (Mn and Mg) into ilmenite and trivalent ions (Cr, Al, V) into magnetite when the two minerals are associated. This distribution was observed in altered and unaltered magnetite and in primary and secondary ilmenite from Hole 504B extrusives and upper sheeted dikes drilled during ODP Leg 83 (Kempton et al., 1985): Al_2O_3 and Cr_2O_3 concentrations are higher in both altered and unaltered magnetite than in ilmenite, whereas MgO and MnO are higher in both primary and secondary ilmenite than in associated magnetite or titanomagnetite. Vanadium concentrations were not reported. Thus, the variations in major and trace elements observed in the lower sheeted dikes drilled during Legs 137, 140, and 148 are consistent with trends observed in magnetite-ilmenite associations in general, as well as in the extrusives and upper sheeted dikes from Hole 504B.

Particle Size and Magnetic Domain State

Differences in the stabilities to AF demagnetization of natural and artificial remanences carried by magnetite are governed by particle size, the relative proportions of low- and high-coercivity particles, the degree of particle alignment, and the interplay between internal stresses within a particle and magnetostatic interactions between pinned and unpinned domain walls (Heider et al., 1992; Moon and Merrill, 1986; Stacey and Banerjee, 1974; Xu and Merrill, 1990; Xu and Dunlop, 1993). Lowrie and Fuller (1971) demonstrated that the relative stabilities to AF demagnetization of IRM and thermoremanent magnetization (TRM) may be used to evaluate the domain state that predominates in the primary carrier of remanence in a sample, assuming that the primary magnetization is carried by magnetite. For single-domain particles, TRM is more stable than IRM, whereas for multidomain particles, IRM is more stable than TRM. The stability of ARM to AF demagnetization is similar to that of TRM (Johnson et al., 1975; Levi and Merrill, 1976), which enabled the Lowrie-Fuller test to be modified to compare stabilities of ARM and IRM, thereby avoiding problems associated with mineralogical changes caused by heating the samples.

For equidimensional grains, pure magnetite is superparamagnetic when less than about 0.03 μm in diameter, single domain from 0.03 to 0.10 μm in diameter, and typically exhibits multidomain at diameters greater than 0.2 μm (Butler and Banerjee, 1975). Particles larger than typical single-domain grains that show single-domain behavior are considered pseudo-single domain. The single domain threshold increases with Ti content. In addition, domain behavior is affected by the elongation of the particle (Butler and Banerjee, 1975), the structure of the grain, oxidation, or microcracks (Haggerty, 1976; Johnson and Hall, 1978; Henshaw and Merrill, 1980) that may produce regions within a large grain that act as single domains.

The ratio of hysteresis parameters J_{RS}/J_S has been used to distinguish between single-domain and multidomain behaviors: values greater than 0.5 indicate single-domain particles, ratios between about 0.1 and 0.5 represent pseudo-single domain particles, and values less than about 0.1 indicate multidomain or superparamagnetic particles (Stoner and Wohlfarth, 1948; Day et al., 1977; Thompson and Oldfield, 1986). Although domain state is not a direct measure of particle size, the ratios may provide some indication of relative changes in domain behavior that reflect changes in particle size.

Samples for which stability to AF demagnetization of ARM and IRM were compared are indicated by an asterisk in Table 2. In all samples, ARM is more stable to demagnetization than IRM, which would indicate that the remanence carrier is single domain. However, the Lowrie-Fuller test, designed for pure equidimensional magnetite, may not be valid for magnetite exsolution lamellae relatively enriched in V_2O_3, Al_2O_3, and Cr_2O_3.

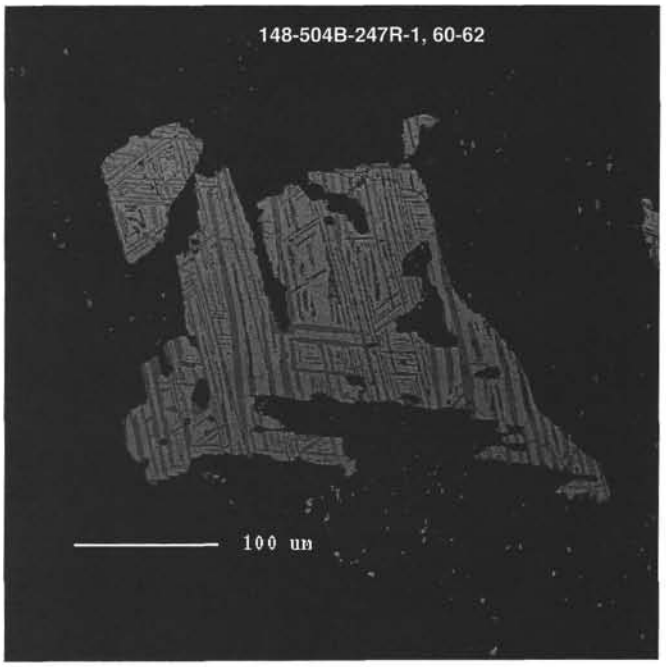

Figure 5. Backscattered electron image of Sample 148-504B-247R-1, 60–62 cm. Dark bands represent ilmenite lamellae and lighter colored bands represent magnetite lamellae.

On the basis of hysteresis parameters, some samples from Hole 504B analyzed in this study exhibit either pseudo-single domain behavior, whereas other samples display behavior that is either multidomain or superparamagnetic (Table 1). Individual lamellae within the magnetite/ilmenite intergrowths observed by reflected light and electron microprobe analysis are thin, often less than one micron in width, and often broken into smaller regions by alteration to titanite or a high-titanium mineral. Thus, although the primary titanomagnetite grain may have been multidomain, after exsolution and subsequent hydrothermal alteration, the coherent magnetic domains have been reduced to the pseudo-single domain or superparamagnetic size regions.

Hole 896A

NRM and Susceptibility

Figure 7 illustrates the variation of NRM and susceptibility with depth in Hole 896A. In the upper part of the hole the intensity of natural remanence is high (shipboard samples: 11.9 A/m; this study: 8.18 A/m), the median destructive field is high (shipboard samples: 22.6 mT; this study: 18.6 mT), and the bulk susceptibility is relatively low (shipboard samples: 0.015 SI; this study: 0.017 SI). In the lower part of the hole, NRM intensity is lower (shipboard samples = 3.9 A/m; this study = 1.45 A/m), median destructive fields are lower (shipboard samples = 12.3 mT; this study = 13.1 mT), and bulk susceptibility values are higher (shipboard samples = 0.033 SI; this study = 0.038 SI). Maximum susceptibility values occur in Units 31–36 (365–407.7 mbsf), which are massive flows that contain large, euhedral titanomaghemites (Fig. 6B, C).

Furuta and Levi (1983) observed similar trends in NRM, MDF and susceptibility data in the Hole 504B extrusive sequence. The change in magnetic properties in Hole 504B occurred below Core 69-

504B-9R, at 332.2 mbsf. Furuta and Levi (1983) attributed these trends to the predominance of pillow units above and massive flows below 332.2 mbsf.

IRM and ARM

In both pillows and massive units from Hole 896A, shipboard isothermal remanent magnetism (IRM) acquisition studies indicate that the rocks generally saturate in applied fields between 70 and 200 mT, consistent with single-domain titanomagnetite and/or titanomaghemite as the carrier of remanence (Alt, Kinoshita, Stokking, et al., 1993). Some samples from massive flows saturated in fields greater than 200 mT, indicating the presence of a higher coercivity mineral, probably hematite (Alt, Kinoshita, Stokking, et al., 1993).

Magnetic Oxide Petrography and Chemistry

Low-temperature oxidation of primary titanomagnetite produced titanomaghemite with shrinkage cracks which were observed in all thin sections from Hole 896A that were analyzed with the electron microprobe. When plotted on a ternary diagram (FeO, TiO_2, 0.5 Fe_2O_3), weight percent data from all samples analyzed failed to fall on the Fe_3O_4–Fe_2TiO_4 join, thus are titanomaghemite (cation-deficient nonstoichiometric spinels; Waychunas, 1991). Groundmass oxidation percentages (Table 3) are from the "Alteration Log" developed by Leg 148 shipboard petrologists (Alt, Kinoshita, Stokking, et al., 1993). Two microprobed samples are from the upper section, in which pillows are predominant. Sample 148-896A-8R-1, 74–76 cm, is a moderately phyric plagioclase-olivine pillow basalt. Titanomaghemite grains are cruciform and subhedral to euhedral, and are less than 5 µm. Total oxidation (yellow-orange-red) of groundmass is 95%. Numerous shrinkage cracks are present and are spaced from <1 to <5 µm apart. Sample 148-896A-11R-1, 91–93 cm, is a moderately phyric plagioclase-olivine pillow basalt containing subhedral titanomaghemite up to 10 µm in diameter. Shrinkage cracks divide the grains into regions <1 to 5 µm in size.

Five microprobed samples are from the lower section, dominated by massive units. Sample 148-896A-24R-1, 111–113 cm, is a massive moderately phyric plagioclase-olivine basalt with subhedral titanomaghemite laths ranging up to 100 × 40 µm in size. Groundmass appears unoxidized; on board ship, the rock was described as gray and fresh-looking (Alt, Kinoshita, Stokking, et al., 1993). Shrinkage cracks are well developed in titanomaghemite and are spaced from 2 to >10 µm apart. Sample 148-896A-24R-3, 94–96 cm, is a massive moderately phyric plagioclase-olivine basalt containing subhedral laths of titanomaghemite up to 40 µm across. Abundant shrinkage cracks break the titanomaghemite grain into regions from <1 to 5 µm across. Reddish oxidative alteration is extensive: oxidation of groundmass is 100%. Sample 148-896A-24R-4, 84–86 cm, is a massive moderately phyric plagioclase-olivine basalt with cruciform and skeletal grains of maghemite up to 30 µm in diameter. The sample contains red and red-brown oxidative halos. Total oxidation of groundmass is 80%. Well-developed shrinkage cracks divide the grains into regions from <1 to 10 µm across. Sample 148-896A-29R-1, 115–117 cm, is a moderately phyric olivine-plagioclase basalt with euhedral to subhedral maghemite laths up to 60 µm in size. Total oxidation of groundmass is 85% and some reddish oxidative alteration halos are present. Shrinkage cracks are numerous and break the grains into regions ranging in size from <1 to 5 µm. Sample 148-896A-30R-1, 134–136 cm, is a moderately phyric olivine-plagioclase pillow basalt containing cruciform maghemite less than 5 µm in diameter. Total oxidation of groundmass is 10%. Shrinkage cracks are abundant, well developed, and break the grain into submicron-sized regions.

Ulvöspinel content (Table 7) in titanomaghemite ranges from about 0.217 to 0.647, with a mean of 0.508. The highest values are from Unit 36: the massive basalt containing large euhedral titanomaghemites (Fig. 6B, C). The lowest values are from pillow units in the upper part of Hole 896A.

Concentrations of V_2O_3 (0.185–1.227 wt%) and Cr_2O_3 (below detection limit to 0.131 wt%, mean = 0.064 wt%) are similar to those measured in magnetite lamellae from Hole 504B samples. Aluminum is relatively enriched in Hole 896A titanomaghemite, ranging from 0.807 to 3.586 wt% and averaging 1. 697 wt%. The concentration of MnO (0.153–3.367 wt%; mean = 1.257 wt%) is similar to that in ilmenite lamellae in Hole 504B intergrowths; however, that of MgO is somewhat higher (0.08–2.165 wt%; mean = 0.577 wt%).

Particle Size and Magnetic Domain State

As for samples from Hole 504B, all samples from Hole 896A for which stability to AF demagnetization of ARM and IRM were compared exhibited behavior characteristic of single domain grains (Figure 4). Again, the Lowrie-Fuller test may not be valid: the carrier of remanence in Hole 896A samples is titanomaghemite, relatively enriched in several trivalent and divalent cations, rather than pure magnetite. Grain morphologies vary from cruciform to euhedral but are rarely equidimensional.

Hysteresis parameters determined from Hole 896A are highly variable, reflecting the range of grain sizes and morphologies and possibly the density and abundance of shrinkage cracks as well. Samples from pillow units (Unit 14: Samples 148-896A-8R-1, 74–76 cm, and 11R-1, 91–93 cm; Unit 51: Sample 148-896A-30R-1, 134–136 cm) fall within the range characteristic of either superparamagnetic or multidomain behavior. The cruciform habit and abundant and dense shrinkage cracks of titanomaghemite within the pillow units make it unlikely that the predominant carrier is multidomain. Many submicron regions were observed during electron microanalysis, indicating the presence of at least some superparamagnetic material (Fig. 6E).

Samples from the massive basalt of Unit 36 also exhibit behavior that may either be superparamagnetic or multidomain. Titanomaghemite grains in this unit are large and euhedral and contain relatively few shrinkage cracks (Fig. 6B, C); hence, they are probably multidomain.

CONCLUSIONS

Samples of lowermost sheeted dikes from Hole 504B recovered during Leg 148 contain low-titanium magnetite, produced during high-temperature deuteric oxidation of primary titanomagnetite to intergrowths of magnetite and ilmenite. Varying degrees of hydrothermal alteration has replaced some or all ilmenite lamellae by titanite and/or a high-titanium mineral (anatase or rutile) and some iron has been lost.

The variability in the amount of magnetizable material produced by differing degrees of hydrothermal alteration of the samples of lowermost sheeted dikes from Hole 504B results in the wide variation in rock magnetic properties observed in this suite of samples, as observed by Pariso and Johnson (1991) and Pariso et al. (1995) in upper portions of the sheeted dike complex.

The ratio of saturation remanence to saturation magnetization in samples of lowermost sheeted dikes from Hole 504B is consistent with pseudo-single-domain behavior.

Magnetite lamellae in Hole 504B magnetite/ilmenite intergrowths from lowermost sheeted dikes are enriched in the trivalent oxides Cr_2O_3 (mean = 0.076 wt%), Al_2O_3 (mean = 0.566 wt%), and V_2O_3 (mean = 0.757 wt%), whereas divalent oxides are concentrated in ilmenite lamellae (mean MnO = 1.997 wt% and mean MgO = 0.073 wt%).

The primary carrier of remanence in volcanic samples recovered from Hole 896A is titanomaghemite produced by low-temperature oxidation of primary titanomagnetite.

Table 7. Major- and trace-element analyses of titanomaghemite in Hole 896A samples.

Core, section, interval (cm)	SiO_2	TiO_2	Al_2O_3	V_2O_3	Cr_2O_3	MnO	NiO	ZnO	MgO	CaO	FeO	Fe_2O_3	Total	Fe/Ti	*X*
148-896A-															
8R-1, 74–76a	0.167	9.674	3.586	0.674	0.063	0.397	0.000	0.129	1.181	0.294	37.642	44.367	98.174	10.359	0.264
8R-1, 74–76a	0.430	9.527	3.506	0.661	0.075	0.377	0.000	0.091	1.366	0.283	38.114	45.315	99.745	10.698	0.256
8R-1, 74–76a	0.287	11.228	3.050	0.532	0.059	0.452	0.046	0.194	1.107	0.235	39.083	41.602	97.875	8.806	0.306
8R-1, 74–76b	0.134	12.018	2.784	0.475	0.039	0.494	0.021	0.019	0.816	0.308	40.331	41.283	98.722	8.331	0.322
8R-1, 74–76b	0.188	12.522	3.041	0.455	0.075	0.447	0.055	0.107	0.761	0.287	40.719	39.287	97.944	7.851	0.339
8R-1, 74–76c	0.299	17.285	2.694	0.515	0.051	0.539	0.000	0.141	0.326	0.378	45.398	29.256	96.882	5.365	0.471
8R-1, 74–76d	0.149	11.303	3.068	0.630	0.096	0.549	0.002	0.148	1.386	0.235	38.704	42.164	98.434	8.762	0.307
11R-1, 91–93a	0.159	10.078	1.149	0.602	0.037	0.284	0.042	0.076	1.252	0.435	37.268	46.298	97.680	10.118	0.270
11R-1, 91–93b	0.086	11.823	1.883	0.672	0.055	0.227	0.081	0.046	1.853	0.186	38.631	43.064	98.607	8.456	0.317
11R-1, 91–93b	0.097	10.934	2.019	0.815	0.110	0.219	0.044	0.042	2.035	0.117	38.078	45.328	99.838	9.319	0.291
11R-1, 91–93b	0.173	10.326	2.141	0.862	0.064	0.183	0.051	0.004	2.072	0.138	37.334	45.572	98.920	9.802	0.278
11R-1, 91–93b	0.084	9.717	2.221	0.817	0.097	0.153	0.118	0.000	2.165	0.125	36.931	47.871	100.300	10.637	0.258
11R-1, 91–93b	0.110	9.404	2.199	0.853	0.099	0.224	0.083	0.091	2.082	0.111	36.465	47.837	99.558	10.922	0.252
11R-1, 91–93c	0.132	8.122	1.958	0.878	0.103	0.217	0.118	0.000	1.715	0.257	35.549	49.999	99.048	12.809	0.217
11R-1, 91–93c	0.195	9.172	2.053	0.934	0.110	0.197	0.000	0.049	1.846	0.210	36.596	47.762	99.124	11.208	0.246
11R-1, 91–93c	0.161	9.182	2.264	0.992	0.131	0.186	0.000	0.000	1.929	0.227	36.334	47.163	98.569	11.083	0.248
11R-1, 91–93c	0.166	10.306	1.726	0.675	0.076	0.173	0.002	0.141	1.565	0.284	37.754	46.010	98.879	9.923	0.275
11R-1, 91–93d	0.198	13.916	2.072	0.721	0.061	0.219	0.028	0.126	1.010	0.213	41.886	37.747	98.197	7.044	0.373
11R-1, 91–93d	0.111	11.999	2.225	0.898	0.094	0.242	0.095	0.228	1.549	0.171	39.528	42.580	99.720	8.382	0.320
11R-1, 91–93d	0.125	13.693	2.079	0.715	0.083	0.226	0.009	0.034	1.235	0.175	41.467	38.644	98.485	7.195	0.366
11R-1, 91–93d	0.255	13.857	2.073	0.765	0.073	0.207	0.042	0.057	1.226	0.216	41.716	37.972	98.458	7.077	0.371
11R-1, 91–93d	0.121	12.132	2.136	0.690	0.081	0.248	0.000	0.004	1.637	0.226	39.212	41.541	98.028	8.158	0.328
24R-1, 111–113a	0.012	20.358	0.996	0.590	0.059	0.495	0.060	0.098	0.180	0.038	49.703	29.036	101.625	4.816	0.516
24R-1, 111–113a	0.098	19.426	1.214	0.550	0.049	0.543	0.000	0.042	0.229	0.014	48.729	29.845	100.739	5.031	0.497
24R-1, 111–113a	0.053	19.087	1.209	0.333	0.018	0.544	0.028	0.045	0.214	0.035	48.219	30.646	100.430	5.134	0.489
24R-1, 111–113a	0.127	18.744	1.180	0.260	0.049	0.507	0.007	0.068	0.201	0.000	48.250	31.550	100.943	5.286	0.477
24R-1, 111–113a	0.149	18.979	0.908	0.238	0.030	0.511	0.005	0.215	0.171	0.051	48.181	31.129	100.567	5.190	0.485
24R-1, 111–113b	0.124	20.706	1.160	0.611	0.045	0.506	0.092	0.098	0.351	0.093	49.604	27.492	100.882	4.643	0.532
24R-1, 111–113b	0.127	21.401	1.010	0.544	0.025	0.499	0.000	0.011	0.353	0.074	50.285	26.109	100.438	4.458	0.550
24R-1, 111–113b	0.092	20.822	1.150	0.628	0.084	0.508	0.005	0.083	0.392	0.044	49.671	27.114	100.592	4.600	0.536
24R-1, 111–113b	0.102	20.653	1.150	0.700	0.072	0.510	0.062	0.076	0.369	0.116	49.045	26.508	99.363	4.564	0.539
24R-1, 111–113c	0.141	19.835	0.834	0.461	0.020	0.436	0.000	0.185	0.231	0.085	49.030	29.622	100.881	4.934	0.506
24R-1, 111–113c	0.108	19.882	0.873	0.330	0.027	0.459	0.009	0.166	0.223	0.024	49.116	29.699	100.917	4.932	0.506
24R-1, 111–113d	0.078	20.024	0.950	0.185	0.039	0.547	0.000	0.166	0.205	0.019	48.967	29.076	100.256	4.851	0.513
24R-1, 111–113d	0.188	19.715	1.174	0.268	0.000	0.532	0.048	0.110	0.252	0.038	49.071	29.757	101.153	4.974	0.502
24R-1, 111–113d	0.113	20.048	1.085	0.321	0.005	0.569	0.021	0.083	0.241	0.013	49.480	29.669	101.649	4.913	0.507
24R-1, 111–113d	0.065	20.147	0.947	0.307	0.000	0.518	0.000	0.159	0.224	0.024	49.056	28.777	100.224	4.810	0.516
24R-1, 111–113d	0.224	19.800	0.997	0.279	0.030	0.530	0.041	0.019	0.353	0.092	48.972	29.595	100.932	4.937	0.505
24R-1, 111–113e	0.149	20.317	1.047	0.472	0.020	0.459	0.000	0.110	0.152	0.035	49.680	28.200	100.642	4.777	0.519
24R-1, 111–113e	0.146	20.428	1.256	0.429	0.049	0.512	0.129	0.045	0.238	0.000	49.461	27.482	100.176	4.696	0.527
24R-1, 111–113e	0.059	20.326	1.362	0.654	0.085	0.489	0.000	0.000	0.284	0.019	49.592	28.021	100.892	4.759	0.521
24R-1, 111–113e	0.094	20.303	1.280	0.669	0.084	0.469	0.030	0.155	0.268	0.051	49.090	27.276	99.769	4.690	0.527
24R-1, 111–113e	0.153	19.916	1.242	0.730	0.047	0.586	0.034	0.253	0.344	0.068	48.730	28.555	100.658	4.832	0.514
24R-3, 94–96a	0.319	22.277	1.674	0.962	0.117	2.444	0.000	0.221	0.219	0.126	48.492	20.427	97.278	3.883	0.614
24R-3, 94–96a	0.145	22.958	1.709	0.970	0.082	2.508	0.000	0.141	0.221	0.062	48.942	19.416	97.154	3.742	0.633
24R-3, 94–96a	0.175	23.081	1.704	1.032	0.089	2.593	0.044	0.141	0.253	0.024	49.224	19.630	97.989	3.748	0.632
24R-3, 94–96a	0.343	22.511	1.762	0.954	0.076	2.647	0.032	0.156	0.209	0.056	48.828	20.183	97.757	3.849	0.619
24R-3, 94–96a	0.131	22.890	1.401	0.813	0.080	2.583	0.016	0.327	0.080	0.084	48.617	19.765	96.787	3.752	0.631
24R-3, 94–96b	0.194	22.209	1.627	0.880	0.064	2.442	0.030	0.217	0.194	0.057	48.343	21.004	97.260	3.916	0.610
24R-3, 94–96b	0.149	22.336	1.522	0.794	0.076	2.528	0.000	0.103	0.154	0.062	48.563	21.230	97.517	3.918	0.610
24R-3, 94–96b	0.852	22.365	1.676	0.660	0.100	2.416	0.032	0.137	0.900	0.022	48.315	19.425	96.900	3.805	0.624
24R-3, 94–96b	0.126	21.766	1.260	0.593	0.061	2.162	0.000	0.106	0.124	0.030	48.297	22.652	97.176	4.081	0.590
24R-3, 94–96c	0.133	23.443	1.690	0.623	0.079	2.424	0.035	0.213	0.413	0.102	48.967	18.899	97.020	3.640	0.647
24R-3, 94–96c	0.236	23.208	1.922	0.904	0.057	2.299	0.062	0.114	0.527	0.068	49.219	19.149	97.766	3.704	0.638
24R-3, 94–96c	0.086	22.997	2.141	0.908	0.114	1.535	0.000	0.194	0.844	0.064	49.122	19.715	97.719	3.761	0.630
24R-3, 94–96c	0.115	21.857	2.508	0.977	0.104	0.927	0.058	0.198	1.039	0.080	48.490	21.657	98.009	4.022	0.597
24R-3, 94–96c	0.324	20.666	2.943	1.227	0.097	1.066	0.062	0.145	1.224	0.129	47.065	22.290	97.238	4.200	0.577
24R-3, 94–96d	0.317	23.208	1.522	0.845	0.078	2.438	0.000	0.281	0.325	0.073	49.383	19.474	97.944	3.729	0.634
24R-3, 94–96d	0.265	23.240	1.675	0.789	0.063	2.592	0.037	0.194	0.192	0.078	49.171	18.729	97.025	3.675	0.642
24R-3, 94–96d	0.122	23.668	1.437	0.785	0.041	2.595	0.030	0.209	0.188	0.059	49.567	19.009	97.710	3.644	0.646
24R-3, 94–96d	0.458	22.747	1.492	0.586	0.103	2.550	0.053	0.103	0.203	0.025	49.223	19.903	97.446	3.817	0.623
24R-3, 94–96d	0.211	23.237	1.168	0.641	0.073	2.648	0.025	0.175	0.102	0.133	49.054	19.571	97.038	3.711	0.637
24R-3, 94–96e	0.186	21.908	1.561	0.414	0.049	2.356	0.000	0.217	0.156	0.030	48.545	22.831	98.253	4.078	0.591
24R-3, 94–96e	0.253	22.006	1.411	0.621	0.043	2.390	0.032	0.080	0.200	0.065	48.301	21.711	97.113	3.987	0.602
24R-3, 94–96e	0.178	21.787	1.383	0.645	0.062	2.135	0.000	0.375	0.221	0.014	48.604	23.530	98.935	4.142	0.583
24R-3, 94–96e	0.252	21.575	1.328	0.601	0.054	2.400	0.000	0.065	0.447	0.081	47.642	23.062	97.506	4.100	0.588
24R-3, 94–96e	0.135	21.794	1.603	0.553	0.066	2.072	0.016	0.175	0.227	0.294	47.861	22.149	96.945	4.023	0.597
24R-3, 94–96f	0.075	22.057	1.502	0.688	0.058	2.330	0.016	0.148	0.189	0.029	48.450	22.372	97.915	4.021	0.597
24R-3, 94–96f	0.303	22.484	1.591	0.852	0.088	2.637	0.035	0.262	0.129	0.024	48.752	20.483	97.640	3.865	0.617
24R-3, 94–96f	0.069	22.103	1.517	0.965	0.098	2.426	0.002	0.311	0.240	0.040	48.288	22.239	98.298	3.996	0.600
24R-3, 94–96f	0.389	21.429	1.326	0.813	0.060	2.353	0.000	0.129	0.176	0.097	48.024	22.531	97.327	4.122	0.586
24R-3, 94–96f	0.387	22.236	1.684	0.820	0.082	2.190	0.000	0.107	0.317	0.049	48.951	20.794	97.617	3.936	0.608
24R-3, 94–96g	0.099	22.262	1.487	0.658	0.085	2.270	0.000	0.076	0.231	0.078	48.314	21.145	96.705	3.912	0.611
24R-3, 94–96g	0.092	21.764	1.547	0.485	0.040	2.225	0.037	0.201	0.196	0.064	48.276	23.271	98.197	4.113	0.587
24R-3, 94–96g	0.160	20.982	1.371	0.473	0.036	1.862	0.009	0.255	0.246	0.060	47.882	24.868	98.205	4.330	0.563
24R-3, 94–96h	0.173	21.411	2.173	1.087	0.102	1.252	0.028	0.125	0.557	0.051	48.864	22.905	98.728	4.196	0.577
24R-3, 94–96h	0.275	20.994	2.113	1.154	0.101	1.553	0.053	0.129	0.548	0.116	47.790	22.555	97.380	4.194	0.578
24R-3, 94–96i	0.162	21.573	1.439	0.618	0.067	2.285	0.051	0.160	0.200	0.088	47.618	22.368	96.629	4.061	0.593
24R-3, 94–96i	0.105	22.655	1.620	0.732	0.076	1.949	0.002	0.175	0.240	0.067	49.266	20.862	97.749	3.884	0.614
24R-3, 94–96i	0.248	22.553	1.624	0.635	0.066	2.521	0.000	0.148	0.118	0.078	48.923	20.631	97.545	3.870	0.616
24R-3, 94–96i	0.908	22.093	1.668	0.540	0.030	2.461	0.035	0.179	0.536	0.059	48.629	19.982	97.120	3.900	0.612
24R-4, 84–86a	0.388	22.362	1.777	0.972	0.080	1.719	0.030	0.102	0.293	0.122	49.776	20.920	98.541	3.968	0.604
24R-4, 84–86a	0.073	22.665	1.562	0.565	0.072	1.898	0.002	0.247	0.087	0.041	49.477	21.079	97.768	3.906	0.612
24R-4, 84–86a	0.106	22.553	1.575	0.551	0.000	1.863	0.000	0.100	0.100	0.081	49.597	21.483	98.010	3.953	0.606
24R-4, 84–86a	0.206	22.218	1.912	0.860	0.111	1.497	0.030	0.232	0.289	0.027	49.406	20.985	97.773	3.975	0.603
24R-4, 84–86b	0.126	19.519	2.676	1.207	0.089	0.606	0.113	0.000	1.319	0.051	46.618	26.324	98.649	4.657	0.530
24R-4, 84–86b	0.193	18.835	2.630	1.079	0.119	0.351	0.042	0.000	1.490	0.200	45.927	27.719	98.585	4.865	0.512
24R-4, 84–86b	0.171	18.000	2.585	1.074	0.060	0.300	0.000	0.091	1.525	0.240	44.659	28.721	97.426	5.064	0.495

Table 7 (continued).

Core, section, interval (cm)	SiO_2	TiO_2	Al_2O_3	V_2O_3	Cr_2O_3	MnO	NiO	ZnO	MgO	CaO	FeO	Fe_2O_3	Total	Fe/Ti	*X*
24R-4, 84–86b	0.130	21.060	1.294	0.349	0.007	1.138	0.058	0.152	0.142	0.054	48.905	25.116	98.406	4.391	0.557
24R-4, 84–86b	0.390	20.326	1.099	0.213	0.031	1.743	0.065	0.179	0.110	0.138	47.586	25.705	97.586	4.499	0.546
24R-4, 84–86b	0.170	20.877	1.354	0.237	0.005	1.527	0.000	0.159	0.124	0.040	48.461	25.329	98.283	4.413	0.554
24R-4, 84–86c	0.535	21.849	1.537	0.764	0.047	1.626	0.000	0.068	0.211	0.084	49.844	22.199	98.764	4.133	0.584
24R-4, 84–86c	0.385	20.386	1.392	0.412	0.011	1.534	0.000	0.201	0.140	0.075	48.191	25.558	98.285	4.516	0.544
24R-4, 84–86c	0.029	20.605	1.311	0.351	0.000	1.223	0.000	0.220	0.163	0.062	48.387	26.606	98.957	4.539	0.542
24R-4, 84–86c	0.111	22.450	1.361	0.693	0.071	1.261	0.014	0.118	0.249	0.070	50.092	22.346	98.836	4.044	0.595
24R-4, 84–86c	0.132	22.129	1.352	0.573	0.068	0.950	0.000	0.129	0.276	0.062	49.890	22.590	98.151	4.104	0.588
24R-4, 84–86d	0.150	22.442	1.921	0.710	0.067	1.335	0.000	0.179	0.401	0.146	49.576	21.207	98.133	3.957	0.605
24R-4, 84–86d	0.592	22.131	1.196	0.535	0.058	1.682	0.000	0.228	0.278	0.135	49.466	21.546	97.846	4.024	0.597
24R-4, 84–86d	0.101	22.402	2.186	0.775	0.071	0.841	0.071	0.049	0.400	0.072	50.119	20.915	98.003	3.980	0.602
29R-1, 115–117a	0.248	20.692	1.774	0.629	0.066	2.265	0.028	0.137	0.173	0.111	47.635	24.753	98.511	4.369	0.559
29R-1, 115–117a	0.153	19.386	1.756	0.698	0.074	1.195	0.023	0.125	0.290	0.057	47.313	27.577	98.647	4.811	0.516
29R-1, 115–117a	0.213	21.034	2.161	0.846	0.059	1.845	0.000	0.034	0.222	0.126	48.188	23.002	97.730	4.235	0.573
29R-1, 115–117b	0.081	18.076	1.622	0.541	0.053	0.941	0.048	0.068	0.631	0.068	45.701	30.763	98.594	5.248	0.480
29R-1, 115–117b	0.110	17.865	1.585	0.560	0.039	0.789	0.062	0.053	0.751	0.024	45.598	31.286	98.722	5.337	0.473
29R-1, 115–117b	0.889	17.134	2.001	0.989	0.090	0.951	0.051	0.042	0.957	0.123	45.299	29.657	98.182	5.432	0.466
29R-1, 115–117c	0.124	14.643	1.554	0.719	0.080	0.398	0.046	0.023	0.697	0.032	43.426	37.934	99.676	6.846	0.382
29R-1, 115–117c	0.045	14.043	1.743	0.684	0.091	0.413	0.060	0.049	0.877	0.033	42.463	39.173	99.675	7.152	0.368
29R-1, 115–117c	0.169	14.463	1.400	0.650	0.042	0.741	0.000	0.034	0.401	0.059	43.090	37.623	98.673	6.876	0.381
29R-1, 115–117c	0.216	16.003	0.807	0.640	0.058	0.735	0.076	0.034	0.293	0.037	44.613	35.184	98.696	6.161	0.419
29R-1, 115–117c	0.237	13.987	1.728	0.610	0.074	0.500	0.055	0.042	0.757	0.086	42.473	38.366	98.915	7.114	0.370
30R-1, 134–136a	0.650	19.901	1.777	0.559	0.048	3.367	0.051	0.179	0.189	0.527	44.983	23.834	96.065	4.316	0.564
Max	0.908	23.668	3.586	1.227	0.131	3.367	0.129	0.375	2.165	0.527	50.285	49.999	101.649	12.809	0.647
Min	0.012	8.122	0.807	0.185	0.000	0.153	0.000	0.000	0.080	0.000	35.549	18.729	96.065	3.640	0.217
Mean	0.203	18.968	1.697	0.673	0.064	1.257	0.029	0.125	0.577	0.106	46.390	28.484	98.572	5.390	0.508
SD	0.160	4.367	0.565	0.225	0.029	0.900	0.031	0.080	0.561	0.095	4.177	8.745	1.270	2.156	0.120

Notes: Max = maximum, Min = minimum, and SD = standard deviation. Value *X* (ulvöspinel content) explained in text. Lowercase letters appended to centimeter intervals refer to different grains within the same thin section.

The Hole 896A interval may be divided into two zones on the basis of magnetic properties: the section above 390 mbsf, predominantly pillow basalts, is characterized by relatively high NRM intensities, low magnetic susceptibilities, and particle sizes that range from the superparamagnetic to pseudosingle domain regions. Massive units in the section below 390 mbsf exhibit lower NRM intensities, higher magnetic susceptibilities, resulting from magnetic particle sizes that range from single to multidomain.

Ulvöspinel content in titanomaghemites from Hole 896A averages 0.508, and ranges from 0.217 to 0.647. Titanomaghemite appears slightly enriched in Al_2O_3 (mean = 1.697 wt%), Cr_2O_3 (mean = 0.064 wt%), V_2O_3 (mean = 0.673 wt%), MnO (1.257 wt%), and MgO (0.577 wt%).

ACKNOWLEDGMENTS

We thank J. Aguiar and C. Cooper for assistance with data processing. We are grateful to R. Guillemette for his guidance and assistance with the electron microprobe and to J. Allan and J. Gee for advice and assistance with microprobe data processing. We thank D. Merrill for his patient efforts in the TAMU Paleomagnetic Laboratory. We are indebted to R. Musgrave for performing the hysteresis measurements and to K. Verosub for kindly allowing us the use of his equipment at University of California, Davis. We thank Ram Alkaly, UCLA Thin Section Laboratory, for preparing polished thin sections of exceptionally high quality. Constructive reviews by J. Pariso, B. Hausen, J. Alt, and P. Michael considerably improved this manuscript. This research was supported by a grant to L.S. from the U.S. Science Support Program of the Joint Oceanographic Institutions, Inc.

REFERENCES

Ade-Hall, J.M., Khan, M.A., Dagley, P., and Wilson, R.L., 1968. A detailed opaque petrological and magnetic investigation of a single Tertiary lava flow from Skye, Scotland, I. Iron-titanium oxide petrology. *Geophys. J. R. Astron. Soc.*, 16:375–388.

Ade-Hall, J.M., Palmer, H.C., and Hubbard, T.P., 1971. The magnetic and opaque petrological response of basalts to regional hydrothermal alteration. *Geophys. J. R. Astron. Soc.*, 24:137–174.

Alt, J.C., Honnorez, J., Laverne, C., and Emmermann, R., 1986. Hydrothermal alteration of a 1 km section through the upper oceanic crust, Deep Sea Drilling Project Hole 504B: mineralogy, chemistry, and evolution of seawater-basalt interactions. *J. Geophys. Res.*, 91:10309–10335.

Alt, J.C., Kinoshita, H., Stokking, L.B., et al., 1993. *Proc. ODP, Init. Repts.*, 148: College Station, TX (Ocean Drilling Program).

Anderson, R.N., Honnorez, J., Becker, K., Adamson, A.C., Alt, J.C., Emmermann, R., Kempton, P.D., Kinoshita, H., Laverne, C., Mottl, M.J., and Newmark, R.L., 1982. DSDP Hole 504B, the first reference section over 1 km through Layer 2 of the oceanic crust. *Nature*, 300:589–594.

Anderson, R.N., Honnorez, J., Becker, K., et al., 1985. *Init. Repts. DSDP*, 83: Washington (U.S. Govt. Printing Office).

Becker, K., Foss, G., et al., 1992. *Proc. ODP, Init. Repts.*, 137: College Station, TX (Ocean Drilling Program).

Becker, K., Sakai, H., Adamson, A.C., Alexandrovich, J., Alt, J.C., Anderson, R.N., Bideau, D., Gable, R., Herzig, P.M., Houghton, S.D., Ishizuka, H., Kawahata, H., Kinoshita, H., Langseth, M.G., Lovell, M.A., Malpas, J., Masuda, H., Merrill, R.B., Morin, R.H., Mottl, M.J., Pariso, J.E., Pezard, P.A., Phillips, J.D., Sparks, J.W., and Uhlig, S., 1989. Drilling deep into young oceanic crust, Hole 504B, Costa Rica Rift. *Rev. Geophys.*, 27:79–102.

Becker, K., Sakai, H., et al., 1988. *Proc. ODP, Init. Repts.*, 111: College Station, TX (Ocean Drilling Program).

Becker, K., Sakai, H., et al., 1989. *Proc. ODP, Sci. Results*, 111: College Station, TX (Ocean Drilling Program).

Butler, R.F., and Banerjee, S.K., 1975. Theoretical single-domain grain-size range in magnetite and titanomagnetite. *J. Geophys. Res.*, 80:4049–4058.

Cande, S.C., and Kent, D.V., 1992. A new geomagnetic polarity time scale for the Late Cretaceous and Cenozoic. *J. Geophys. Res.*, 97:13917–13951.

Cann, J.R., Langseth, M.G., Honnorez, J., Von Herzen, R.P., White, S.M., et al., 1983. *Init. Repts. DSDP*, 69: Washington (U.S. Govt. Printing Office).

Carmichael, I.S.E., 1967. The iron-titanium oxides of salic volcanic rocks and their associated ferromagnesian silicates. *Contrib. Mineral. Petrol.*, 14:36–64.

Cisowski, S., 1980. The relationship between the magnetic properties of terrestrial igneous rocks and the composition and internal structure of their component Fe-oxide grains. *Geophys. J. R. Astron. Soc.*, 60:107–122.

CRRUST (Costa Rica Rift United Scientific Team), 1982. Geothermal regimes of the Costa Rica Rift, east Pacific, investigated by drilling, DSDP-IPOD Legs 68, 69, and 70. *Geol. Soc. Am. Bull.*, 93:862–875.

Day, R., Fuller, M., and Schmidt, V.A., 1977. Hysteresis properties of titanomagnetites: grain-size and compositional dependence. *Phys. Earth Planet. Inter.*, 13:260–267.

Deer, W.A., Howie, R.A., and Zussman, J., 1962. *Rock-forming Minerals* (Vol. 5): *Non-silicates:* New York (Wiley).

Dick, H.J.B., Erzinger, J., Stokking, L.B., et al., 1992. *Proc. ODP, Init. Repts.*, 140: College Station, TX (Ocean Drilling Program).

Dunlop, D.J., 1969. Hysteretic properties of synthetic and natural monodomain grains. *Philos. Mag.*, 19:329–338.

Evans, M.E., and Wayman, M.L., 1974. An investigation of the role of ultrafine titanomagnetite intergrowths in paleomagnetism. *Geophys. J. R. Astron. Soc.*, 36:1–10.

Furuta, T., and Levi, S., 1983. Basement paleomagnetism of Hole 504B. *In* Cann, J.R., Langseth, M.G., Honnorez, J., Von Herzen, R.P., White, S.M., et al., *Init. Repts. DSDP*, 69: Washington (U.S. Govt. Printing Office), 697–703.

Haggerty, S.E., 1976. Oxidation of opaque mineral oxides in basalts. *In* Rumble, D., III (Ed.), *Oxide Minerals.* Short Course Notes—Mineral. Soc. Am., 3:101–277.

————, 1991. Oxide textures: a mini-atlas. *In* Lindsley, D.H. (Ed.), *Oxide Minerals: Petrologic and Magnetic Significance.* Rev. Mineral., 25:129–219.

Hall, J.M., and Fisher, B.E., 1987. The characteristics and significance of secondary magnetite in a profile through the dike component of the Troodos, Cyprus, ophiolite. *Can. J. Earth Sci.*, 24:2141–2159.

Heider, F., Dunlop, D.J., and Soffel, H.C., 1992. Low-temperature and alternating field demagnetization of saturation remanence and thermoremanence in magnetite grains (0.037 µm to 5 mm). *J. Geophys. Res.*, 97:9371–9381.

Henshaw, R.C., Jr., and Merrill, R.T., 1980. Magnetic and chemical changes in marine sediments. *Rev. Geophys. Space Phys.*, 18:483–504.

Hobart, M.A., Langseth, M.G., and Anderson, R.N., 1985. A geothermal and geophysical survey on the south flank of the Costa Rica Rift: Sites 504 and 505. *In* Anderson, R.N., Honnorez, J., Becker, K., et al., *Init. Repts. DSDP*, 83: Washington (U.S. Govt. Printing Office), 379–404.

Johnson, H.P., and Hall, J.M., 1978. A detailed rock magnetic and opaque mineralogy study of the basalts from the Nazca Plate. *Geophys. J. R. Astron. Soc.*, 52:45–64.

Johnson, H.P., Lowrie, W., and Kent, D.V., 1975. Stability of anhysteretic remanent magnetization in fine and coarse magnetite and maghemite particles. *Geophys. J. R. Astron. Soc.*, 41:1–10.

Kempton, P.D., Autio, L.K., Rhodes, J.M., Holdaway, M.J., Dungan, M.A., and Johnson, P., 1985. Petrology of basalts from Hole 504B, Deep Sea Drilling Project, Leg 83. *In* Anderson, R.N., Honnorez, J., Becker, K., et al., *Init. Repts. DSDP*, 83: Washington (U.S. Govt. Printing Office), 129–164.

Leinen, M., Rea, D.K., et al., 1986. *Init. Repts. DSDP*, 92: Washington (U.S. Govt. Printing Office).

Levi, S., and Merrill, R.T., 1976. A comparison of ARM and TRM in magnetite. *Earth Planet. Sci. Lett.*, 32:171–184.

Lowrie, W., and Fuller, M., 1971. On the alternating field demagnetization characteristics of multidomain thermoremanent magnetization in magnetite. *J. Geophys. Res.*, 76:6339–6349.

Moon, T., and Merrill, R.T., 1986. Magnetic screening in multidomain material. *J. Geomagn. Geoelectr.*, 38:883–894.

Pariso, J.E., and Johnson, H.P., 1991. Alteration processes at Deep Sea Drilling Project/Ocean Drilling Program Hole 504B at the Costa Rica Rift: implications for magnetization of oceanic crust. *J. Geophys. Res.*, 96:11703–11722.

Pariso, J.E., Stokking, L., and Allerton, S., 1995. Rock magnetism and magnetic mineralogy of a 1-km section of sheeted dikes, Hole 504B. *In* Erzinger, J., Becker, K., Dick, H.J.B., and Stokking, L.B. (Eds.), *Proc. ODP, Sci. Results,* 137/140: College Station, TX (Ocean Drilling Program), 253–262.

Rice, P.D., Hall, J.M., and Opdyke, N.D., 1980. Deep Drill 1972: a paleomagnetic study of the Bermuda Seamount. *Can. J. Earth Sci.*, 17:232–243.

Smith, G.M., and Banerjee, S.K., 1986. Magnetic structure of the upper kilometer of the marine crust at Deep Sea Drilling Project Hole 504B, Eastern Pacific Ocean. *J. Geophys. Res.*, 91:10337–10354.

Smith, G.M., Gee, J., and Klootwijk, C.T., 1991. Magnetic petrology of basalts from Ninetyeast Ridge. *In* Weissel, J., Peirce, J., Taylor, E., Alt, J., et al., *Proc. ODP, Sci. Results,* 121: College Station, TX (Ocean Drilling Program), 525–545.

Stacey, F.D., and Banerjee, S.K., 1974. *The Physical Principles of Rock Magnetism.* Dev. Solid Earth Geophys., 5: New York (Elsevier).

Stokking, L.B., Heise, E.A., Pariso, J.E., and Allerton, S.A., 1995. *Data report:* magnetic mineralogy, major- and trace-element geochemistry, and rock magnetic properties of Hole 504B upper crustal rocks. *In* Erzinger, J., Becker, K., Dick, H.J.B., and Stokking, L.B. (Eds.), *Proc. ODP, Sci. Results,* 137/140: College Station, TX (Ocean Drilling Program), 327–338.

Stoner, E.C., and Wohlfarth, E.P., 1948. A mechanism of magnetic hysteresis in heterogeneous alloys. *Philos. Trans. R. Soc. London A*, 240:599.

Thompson, R., and Oldfield, F., 1986. *Environmental Magnetism:* London (Allen and Unwin).

Waychunas, G.A., 1991. Crystal chemistry of oxides and oxyhydroxides. *In* Lindsley, D.H. (Ed.), *Oxide Minerals: Petrologic and Magnetic Significance.* Rev. Mineral., 25:11–68.

Xu, S., and Dunlop, D.J., 1993. Theory of alternating field demagnetization of multidomain grains implications for the origin of pseudo-single domain remanence. *J. Geophys. Res.*, 98:4183–4190.

Xu, S., and Merrill, R.T., 1990. Toward a better understanding of magnetic screening in multidomain grains. *J. Geomagn. Geoelectr.*, 42:637–652.

Date of initial receipt: 15 August 1994
Date of acceptance: 28 February 1995
Ms 148SR-130

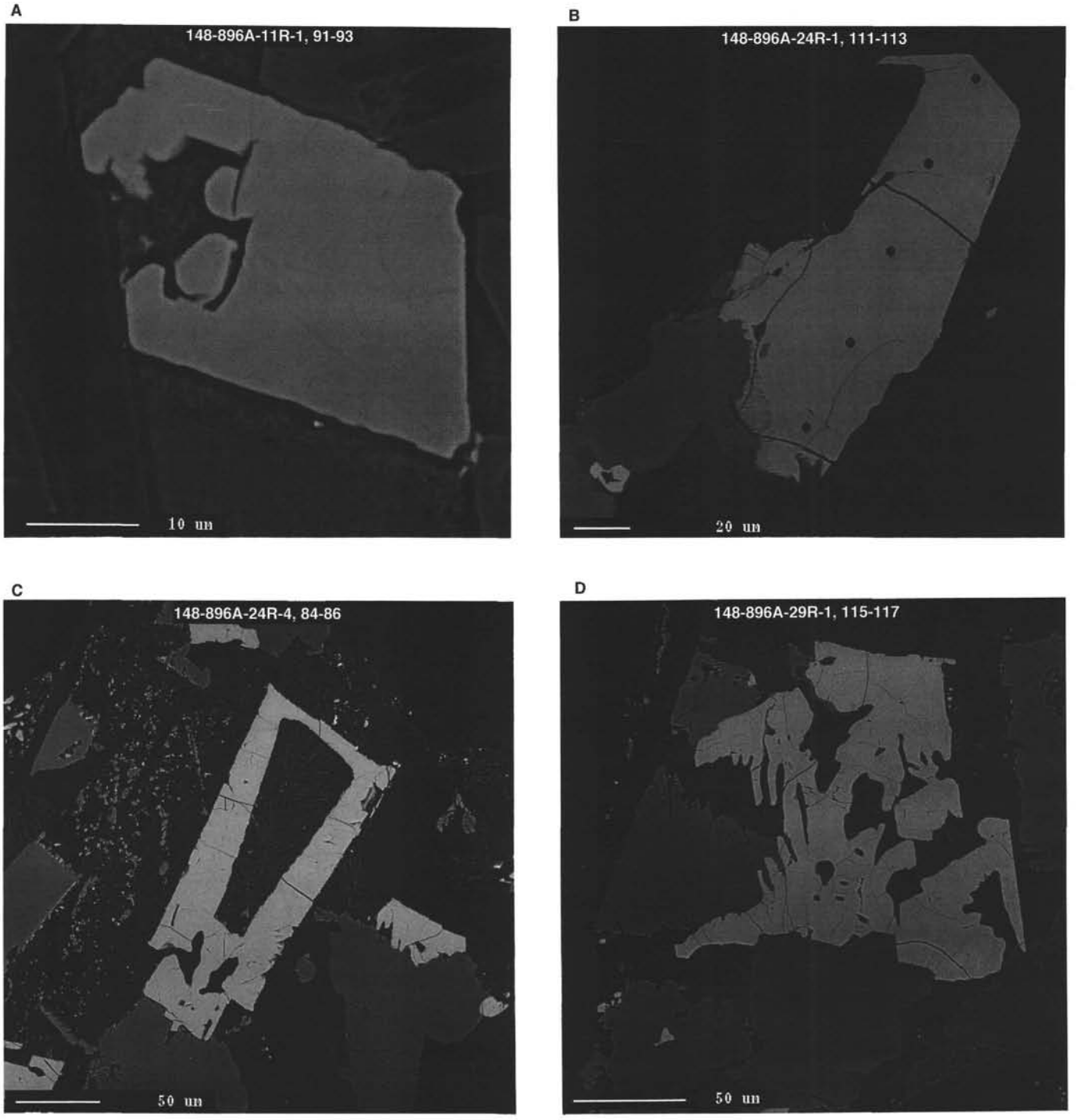

Figure 6. Backscattered electron images. **A.** Sample 148-896A-11R-1, 91–93 cm. The light-colored grain in the center of the image is titanomaghemite. Dark curved lines cutting the titanomaghemite grain are shrinkage cracks. **B.** Sample 148-896A-24R-1, 111–113 cm. The elongate light-colored grain in the center of the image is titanomaghemite. Dark curved lines cutting the titanomaghemite grain are shrinkage cracks. The backscattered electron (BSE) image of this sample was captured after microprobe analyses were performed, whereas the other BSE images presented in Figure 6 were captured before microprobe analyses were conducted. This image, therefore, includes dark spots that were burned in by the microprobe beam. **C.** Sample 148-896A-24R-4, 84–86 cm. The large light-colored grains in the center of the image, in the lower left corner, the upper edge, and adjacent to the central grain are titanomaghemite. Dark curved lines cutting the titanomaghemite grain are shrinkage cracks. **D.** Sample 148-896A-29R-1, 115–117 cm. The large, light-colored, irregularly shaped grain in the center of the image is titanomaghemite. Dark curved lines cutting the titanomaghemite grain are shrinkage cracks. **E.** Sample 148-896A-30R-1, 134–136 cm. The light-colored, irregularly shaped grain (or grain cluster) in the center of the image is titanomaghemite. Dark curved lines cutting the titanomaghemite grains are shrinkage cracks.

E

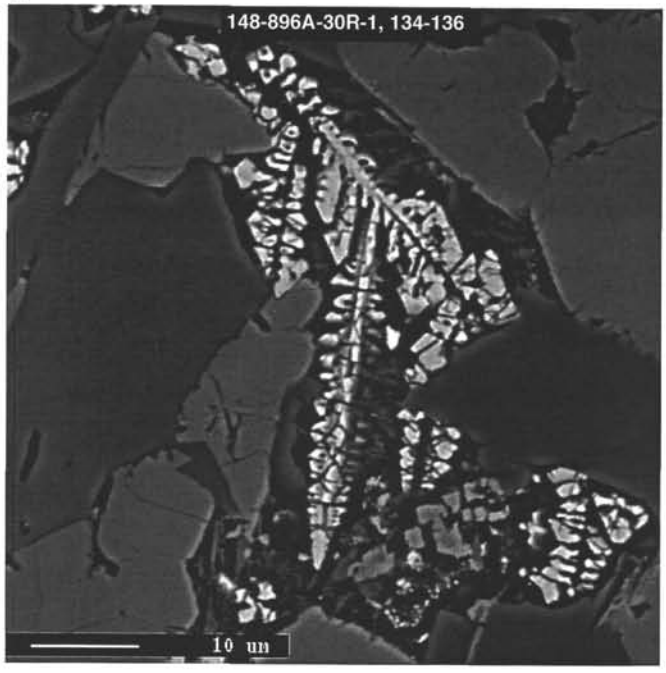

Figure 6 (continued).

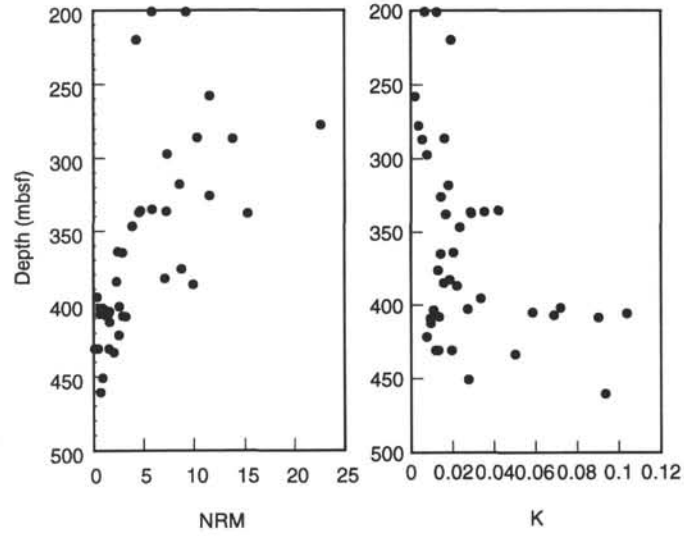

Figure 7. Downhole variation of NRM and susceptibility (K), Hole 896A.